Earth and Space Science

RESEARCH ARTICLE
10.1029/2022EA002447

Alongshore Variable Accretional and Erosional Coastal Foredune Dynamics at Event to Interannual Timescales

Nicholas Cohn[1], Katherine Brodie[1], Ian Conery[1], and Nicholas Spore[1]

[1]Coastal and Hydraulics Laboratory – Field Research Facility, U.S. Army Engineer Research and Development Center, Duck, NC, USA

Key Points:

- Both wind and wave-driven contributions to volumetric dune change are measurable at event scale using mobile terrestrial lidar
- The fastest dune growth rates are generally on sections of coast with the mildest beach slopes
- Anthropogenic activities, including nourishment and sand fencing, have a quantifiable effect on the magnitude and style of dune evolution

Correspondence to:
N. Cohn,
nicholas.t.cohn@gmail.com

Citation:
Cohn, N., Brodie, K., Conery, I., & Spore, N. (2022). Alongshore variable accretional and erosional coastal foredune dynamics at event to interannual timescales. *Earth and Space Science*, *9*, e2022EA002447. https://doi.org/10.1029/2022EA002447

Received 31 MAY 2022
Accepted 27 SEP 2022

Author Contributions:
Conceptualization: Nicholas Cohn
Data curation: Nicholas Cohn, Katherine Brodie, Ian Conery, Nicholas Spore
Formal analysis: Nicholas Cohn, Ian Conery, Nicholas Spore
Funding acquisition: Nicholas Cohn, Katherine Brodie
Investigation: Nicholas Cohn
Methodology: Nicholas Cohn, Katherine Brodie, Ian Conery, Nicholas Spore
Project Administration: Nicholas Cohn
Writing – original draft: Nicholas Cohn
Writing – review & editing: Katherine Brodie, Ian Conery, Nicholas Spore

Abstract Natural and constructed dunes are increasingly being utilized to buffer flooding impacts from storms and rising sea levels along sandy coastlines. However, a lack of data at the appropriate spatial and temporal resolution often precludes isolating the total magnitude, specific timing, and alongshore variability of volumetric coastal dune changes resulting from both wave and wind-driven processes. Here mobile terrestrial lidar data from 46 collections along a 6.5 km stretch of sandy beach and dunes in Duck, NC, USA are used to assess the magnitude and drivers of alongshore variable dune responses between 2012 and 2020. Despite numerous major storm events which impacted the dunes over this time period, the dunes grew volumetrically both in nourished and un-nourished sections of the study site. Growth of the dunes was seasonally and spatially variable with the largest total growth recorded in the Fall, coinciding with a period of frequent windy storms but also the highest total water levels, and along the regions with the lowest gradient β_{beach}. The vertical accretion patterns of these wind-blown sediments are shown to vary depending on the dune management style, specifically, if dunes were not managed, sand fenced, or artificially constructed. Dune erosion also occurred episodically within the study period, with the steepest sloped beach sections likely to be the most impacted during individual storm events.

1. Introduction

Foredunes are common landforms on many sandy beaches that develop from the complex interplay of marine, aeolian, ecological, and anthropogenic processes. The magnitude of accretional inputs to coastal dunes is dependent on wind properties (e.g., Bauer & Davidson-Arnott, 2003; Sherman & Hotta, 1990), sediment availability (de Vries et al., 2014), the influence of beach morphology on fetch lengths and moisture patterns (Bauer et al., 2009; Davidson-Arnott et al., 2018; Sherman & Lyons, 1994), dune grass properties (e.g., Hesp, 1981; Reijers et al., 2020; Zarnetske et al., 2012), and feedbacks of the dune morphology on the local wind field (e.g., Hesp & Smyth, 2019; D. Jackson et al., 2013). Foredune landforms develop slowly from these aeolian inputs, with typical foredune growth rates of under ~15 m^3/m/yr during accretional conditions along much of the world's beaches (e.g., Ciarletta et al., 2019; Cohn et al., 2018; Costas et al., 2020; de Vries et al., 2012; Mathew et al., 2010; Strypsteen et al., 2019). Wave-driven sediment transport may cause a wider range of potential impacts, with some mild storm events being a positive source of sediment supply to the foredune (e.g., Cohn et al., 2018) whereas overwash and inundation events (Sallenger, 2000) commonly destroy entire dune systems (e.g., Feagin & Williams, 2008; Figlus et al., 2011). During collisional events, corresponding to periods when the total water level (TWL) exceeds the dune toe, an erosional scarp feature is often formed (e.g., Davidson et al., 2020; Erikson et al., 2007). Although the elevation and duration of the TWL relative to the dune toe are the primary drivers of the magnitude of dune erosion (e.g., Larson et al., 2004; Palmsten & Holman, 2012), morphologic feedbacks and biotic factors (e.g., Feagin et al., 2015) are also known to influence the scale of dune impacts during storms. These morphologic effects include the role of nearshore sandbars and beach morphology influencing wave setup, incident swash, and infragravity swash contributions to wave runup (e.g., Cohn et al., 2019; Cox et al., 2013), controls of the pre-storm dune face slope on dune erodibility (e.g., de Winter et al., 2015), and the trajectory of the dune toe in response to wave collision (e.g., Overbeck et al., 2017). As these morphologic and environmental conditions can be highly site specific, there can be considerable alongshore variability in dune accretion and erosion over regional scales (Garzon et al., 2022; J. G. Keijsers et al., 2014).

There are increasing efforts to construct dunes on low-lying beach systems around the world for added resilience from storm and sea level rise-related flooding hazards (e.g., Bridges et al., 2015; Morris et al., 2018). These constructed dunes are designed to serve similar functions to natural dunes, with their primary purpose of

serving as a local topographic high to limit overtopping and water-related hazards to low-lying, beach-adjacent infrastructure. There are, however, notable differences in both the protective and ecosystem services that natural vs. artificial dunes provide (e.g., De Battisti & Griffin, 2020). For example, built dunes are often planted with sparse, regularly spaced sprigs that can take numerous years to develop. This is in contrast to the dense vegetation that is characteristic of many natural dune systems that is known to be effective at trapping wind-blown sands (Hesp, 1981, 1989; J. Keijsers et al., 2015), having important implications for subsequent sediment deposition patterns. Sand fences are widely used to aid in the trapping of sand and stabilization of coastal foredunes (Grafals-Soto & Nordstrom, 2009) on both constructed, as well as non-built, dunes. Itzkin et al. (2020) found that the placement of sand fences near the base of the dune resulted in a wider, but less tall, dune complex relative to nearby un-fenced dunes. The details of fence orientation and location additionally play a critical role in determining where and how much sediment is trapped on dunes (e.g., N. L. Jackson & Nordstrom, 2011; Mendelssohn et al., 1991; Miller et al., 2001).

Dune construction is often associated with beach nourishment. Wind-blown fluxes to the dunes have additionally been observed to increase immediately following beach nourishment placement (e.g., Conery, Brodie, Spore, & Walsh, 2020; Kaczkowski et al., 2018). This increase in aeolian transport to the dune is presumably related to either (a) an increased beach fetch on wide, recently constructed beaches, resulting in more frequent saturated transport over the backshore, and/or (b) a larger fraction of fines (relative to the native beach sands) on the beach immediately following beach nourishment that have a lower threshold velocity for the initiation of wind-blown sand transport (Bagnold, 1937). Though these are hypotheses, limited studies have documented these altered aeolian transport dynamics (e.g., van der Wal, 2000) on nourished vs. natural beach systems.

Despite these ecological and morphodynamic processes that are recognized as having an effect on sediment transport and bed elevation change in beach-dune systems, few research studies have explored how natural vs. managed dunes differ in their behavior—likely in part due to the complicated three-dimensional (3D) evolution of these features across a wide range of timescales (days to years). Studies that characterize alongshore variable 3D dune evolution are typically completed using airborne lidar data. These data cover large geographic extents, but for the purposes of most sites are too temporally coarse (e.g., >1 yr sampling intervals) to attribute dynamics to discrete storm events. Root mean square surveying errors for airborne lidar data are generally thought to be ∼0.05–0.3 m, with errors increasing on sloped and vegetated terrains (e.g., Enwright et al., 2018; Hodgson & Bresnahan, 2004). These data often provide sufficient accuracy and resolution for measuring storm-driven erosional patterns in coastal systems, but may be in the noise for measuring the comparatively smaller magnitude accretional processes. Many beach monitoring programs also collect cross-shore transect-based data on monthly to seasonal scale that provides valuable insights into subaerial coastal morphology change. However, transect-based analyses suffer from not being able to characterize the full topographic complexity of coastal dune systems. Over the past decade, the use of structure-from-motion reconstructions of topography using unmanned aerial vehicles (UAV) has become common across coastal and non-coastal areas (Laporte-Fauret et al., 2019; Taddia et al., 2019). However, there remain issues with the detection of the bed surface in (a) heavily vegetated regions which may limit the detection of small-scale aeolian deposition signals within dunes and (b) scalability issues with using UAV systems over large regions due to ground control and line of sight constraints which limits their use generally to the sub-kilometer scale (Brodie, Bruder, Slocum, & Spore, 2019; Renaud et al., 2019).

Terrestrial laser scanning is also increasingly being utilized to provide 3D insights into coastal landform evolution (e.g., Brodie, Conery, Cohn, Spore, & Palmsten, 2019; de Vries et al., 2017; Vos et al., 2017). Tripod-based applications are limited in the geographic domain of surveying, although lidar scanners can also be mounted on vehicles to extend the scales of data collection (Donker et al., 2018; Lim et al., 2013). These mobile terrestrial lidar (MTL) applications have the benefit of being able to cover regional spatial domains with high accuracy, although do have field of view limitations that limits their ability to resolve deposition landward of the dune crest for MTL systems being driven on the beach.

In this study, we present 3D MTL measurements collected along a 6.5 km stretch of coastline in Duck, NC, USA that included a segment with nourished beaches and dunes. Using this data, we quantitatively detail alongshore variability in dune erosion and growth rates in order to decouple the relative morphologic and anthropogenic factors that contribute to the resistance of these features. In this manuscript, Section 2 gives an overview of the field site and the MTL data collection program. Data collected at timescales of days to months apart over a multiyear period are used to quantify the timing, magnitude, and spatial distribution of bed elevation changes

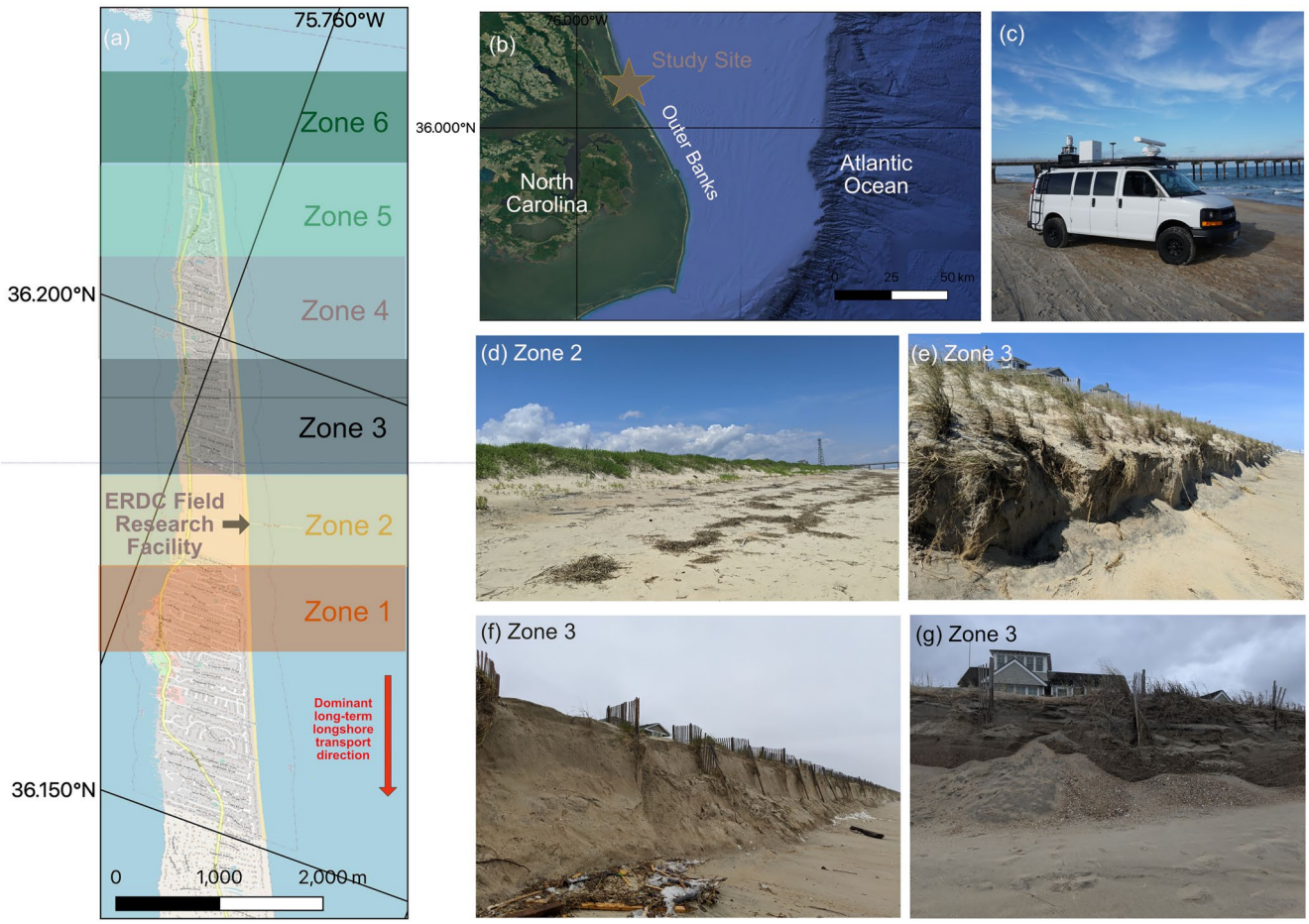

Figure 1. Overview map of the study site location (panels (a–b)), including the alongshore extents of the six zones used in this analysis (panel (a)). Additionally, a pictures of (panel (c)) the CLARIS lidar platform and (panel (d)) a representative section of beach and dune from Zone 2 are shown. Pictures of scarp development at roughly the same location within Zone 3 are shown on 20 September 2019 following Hurricane Dorian (panel (e)), on 18 November 2019 coinciding with a Nor'Easter even (panel (f)), and 7 December 2020 shortly after dune collision from the swells of Hurricane Teddy (panel (g)).

and corresponding volume changes to dunes. The results of these collective morphology data, in the context of environmental and anthropogenic influences, is provided in Section 3. Discussion of the data and the drivers of alongshore and temporally variable dune processes are given in Section 4. Conclusions are provided in Section 5.

2. Field Data Collection and Methods

2.1. Field Site

The Outer Banks is a barrier island chain off of the North Carolina (United States) coast. These islands typically experience numerous collisional events per year from hurricanes or remnants of hurricanes, tropical storms, and extratropical events (e.g., Sallenger et al., 2001). The influence from these storms is commonly non-uniform, with morphologically controlled hotspot beach and dune erosion preferentially threatening certain sites with uncharacteristic offshore (Schupp et al., 2006) or inner surf zone bathymetry (Cohn et al., 2021). These morphologic behaviors have been well documented on the northern Outer Banks, especially via a long-term monitoring program at the U.S. Army Engineer Research and Development Center (ERDC) Field Research Facility (FRF) in Duck, NC (Birkemeier & Forte, 2019; Crowson et al., 1988). Data from the FRF shows a highly 3D beach topography throughout the region that evolves on ~ daily timescales associated with beach cusp evolution (O'Dea & Brodie, 2019), intermittent storm-driven beach and dune erosion (Brodie, Conery, et al., 2019), and prevalent sand mobilization from wind-driven processes that contributes to dune growth (Conery, Brodie, et al., 2020). This study focuses on a 6.5 km stretch of beach within the town of Duck (Figure 1), including the FRF property

Table 1
Management Type by Region

Region	Management type	*Y* range (m)
Zone 1	Partially managed—sand fences	−1,200 to 0
Zone 2	Unmanaged/natural	0–1,000
Zone 3	Constructed—beach and dune nourishment, sand fences	1,000–2,100
Zone 4	Constructed—beach and dune nourishment, sand fences	2,100–3,300
Zone 5	Partially managed—sand fences	3,300–4,300
Zone 6	Partially managed—sand fences	4,300–5,300

(Zone 2 in Figure 1a). The 1 km stretch of coast at the FRF is unique for the region in that, other than access ramps for vehicles, there is no management of the beach or dune system since their construction by the Civilian Conservation Corps in the 1930s (Birkemeier et al., 1984). This includes no sand fencing along this 1 km coastal stretch, as noted in Table 1.

Because there is a negative background erosion rate in the Outer Banks (Armstrong & Lazarus, 2019) that is about −1 m/yr in Duck (Kratzmann et al., 2017), in part due to long-term net longshore transport rates to the south (Inman & Dolan, 1989), many local communities have adopted a policy of active beach and dune nourishment (e.g., Kana & Kaczkowski, 2012). In the Summer of 2017, the town of Duck, NC placed about 1 million m^3 of dredged sediments along a ∼2.5 km stretch of coastline in order to expand useable beach for recreational purposes, buffer impacts of storms, and mitigate long-term erosion trends (CPE, 2017). The initial nourished design template included a wide, flat upper beach and a constructed dune. Sediment for the nourishment was sourced from two offshore borrow sources. The dune was planted with *Ammophila breviligulata* and sand fences were installed in numerous rows within the constructed dune complex. Although the zone of placement of sand within the Town of Duck was limited to 2.5 km, the remainder of the town's coastline, other than the FRF, have installed sand fencing to aid in the trapping of wind-blown sand (Table 1). It is also common for used Christmas trees to be placed and grasses to be planted near the base of the dune throughout managed portions of the study site to aid in additional sand trapping.

2.2. Environmental Forcings

Numerous meteorological and oceanographic instruments are located at the FRF which provide the necessary context for observed morphologic changes within the study bounds. A tide gauge located at end of the FRF pier was used to generate a time series of still water levels (SWL, Figure 2). Wind speeds and directions were collected at a meteorological station also located at the end of the pier at 20 m elevation. Wave heights, periods, and directions were derived from a waverider buoy located in approximately 17 m water depth offshore the study site. Any temporal gaps in the wave time series were supplemented with data from a wave buoy located further offshore Duck in 26 m water depth. To determine the occurrence of wave collision with the dunes, wave runup and TWLs were estimated from the available data. The eight empirically based models for 2% wave runup exceedance level ($R_{2\%}$) included within Leaman et al. (2020) were averaged to generate an hourly record of wave runup. The hourly TWL was calculated as the average $R_{2\%}$ plus the measured SWL from the FRF pier. An example TWL time series assuming a beach slope (β_{beach}) of 0.1 m/m (the average regional β_{beach}) is shown in Figure 2i. Any reference to TWLs at site-specific locations throughout the manuscript utilizes locally measured (spatially variable) β_{beach} in the wave runup calculations. Note that all vertical references to water levels and bed elevation herein are provided in the NAVD88 datum, where mean high water (MHW) is approximately 0.4 m.

2.3. Morphology Data

2.3.1. Coastal Lidar and Radar Imaging System (CLARIS)

The CLARIS is a custom-built mobile surveying platform for coastal environments (Figure 1c). Detailed topographic data has been collected with CLARIS along the Outer Banks study site since 2012. The current iteration of the CLARIS platform, which has been operational since 2017, is built onto a four-wheel drive passenger van.

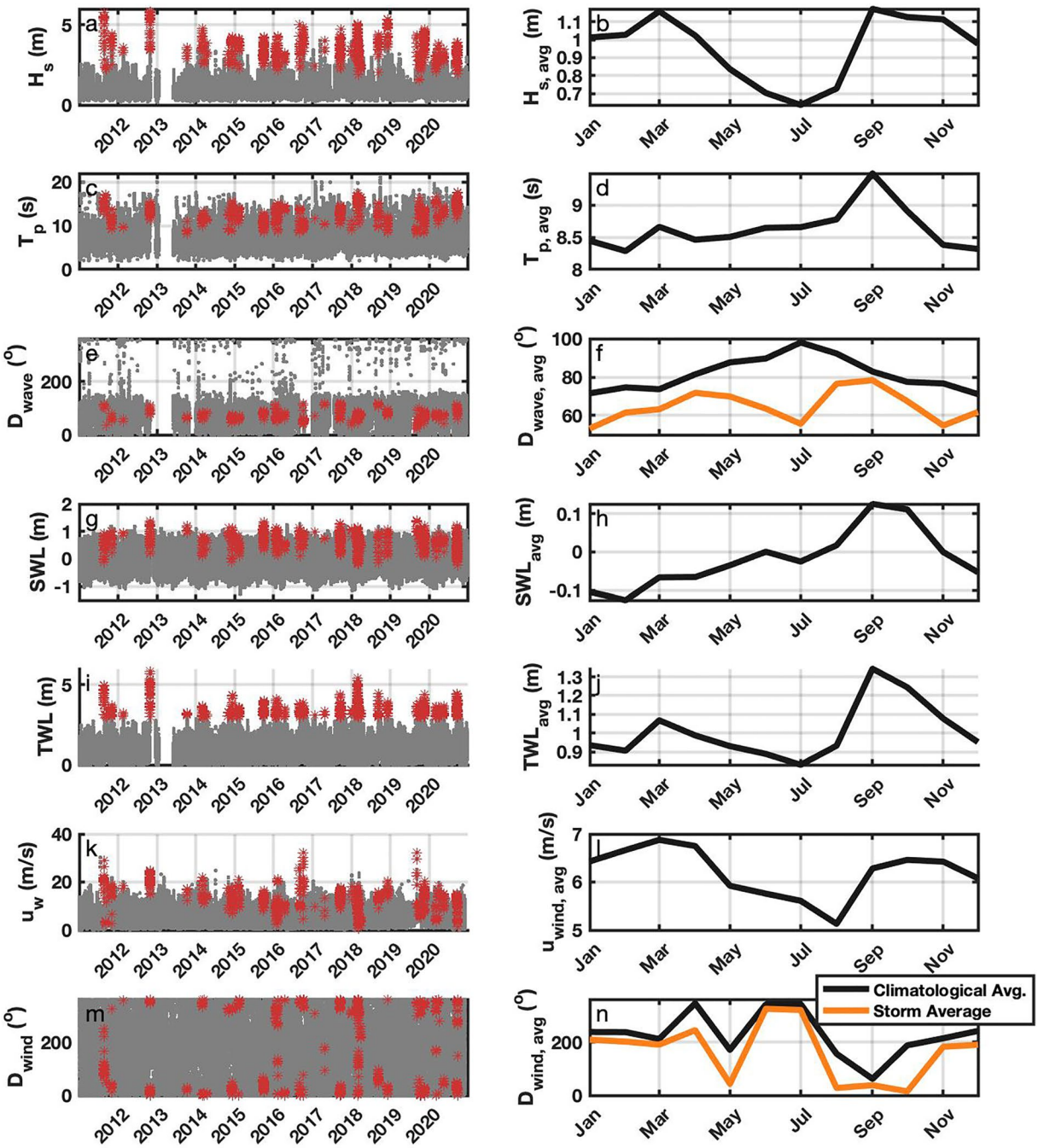

Figure 2. Time series of (a) significant wave height, (c) peak wave period, (e) still water level, (g) total water level (TWL) using β_{beach} of 0.1 m/m, and (i) wind speed. Red dots represent time periods where the estimated average TWL exceeded 3 m, which approximates the regional dune toe elevation as derived from Beuzen (2019). Monthly average values for each environmental variable are also shown in panels (b, d, f, h, and j) as black lines. The average direction of winds when u_w exceeds 8 m/s (approximate threshold velocity for aeolian transport, panel (n)) and waves when significant wave heights exceed 3 m (panel (f)) are also shown as orange lines.

The unit includes a Riegl VZ-2000 lidar scanner which continuously scans to collect high-resolution 3D point clouds of terrain and other objects. The CLARIS system also includes an IX-Blue ATLANS-C inertial navigation system (INS) with an integrated inertial measurement unit, wheel-mounted distance measurement instrument, and global navigation satellite system antennas to allow for precise orientation of the lidar-derived point clouds in real-world space. Previous iterations of CLARIS (<2017) were mounted on different vehicle platforms but included similar instrumentation and data quality, as outlined in Spore and Brodie (2017).

Table 2
Peak Environmental Characteristics of Storms Events With Detailed Pre-/Post-Storm CLARIS Data

Storm name	Time period	Max H_s (m)	Max T_p (s)	Max SWL (m)	Max TWL (m)
Hurricane Jose	September 2017	4.2	14.8	1.29	4.39
Hurricane Dorian	September 2019	4.4[a]	11.3	1.40	3.66
2019 Nor'Easter	November 2019	4.7	14.0	1.21	4.38
Hurricane Teddy	September 2020	3.9	17.7	1.21	4.45

[a]Other FRF wave gauges showed peak H_s exceeding 6 m during this short-lived, energetic hurricane event.

These CLARIS data cover the beach and dune face in high detail and are therefore used to quantify dune evolution in time and space. Based on typical driving speeds (~10 km/hr) and height of the vehicle (~2.5 m), data density is roughly 100 pts/m^2 between overlapping framescans within about 50 m of the van. An analysis of the scanner performance with these settings for resolving beach and dune topography is described in Conery, Cohn, et al. (2020). Mean vertical errors using gridded CLARIS outputs relative to RTK GPS measurements are typically <0.05 m, making the data from this system suitable to resolve both accretional and erosional processes within coastal dunes in locations with sufficient point density. The CLARIS system does have line of sight limitations and cannot measure bed elevation changes near or past the dune crest. Thus, bed elevation change associated with jettation events and other thin layer deposition past the foredune crest (e.g., Hesp & Smyth, 2016; Ollerhead et al., 2013) are not captured by CLARIS.

2.3.2. Collection Time Periods

At least quarterly (four times per year) CLARIS scans are collected in Duck. These surveys are supplemented by occasional pre- and post-storm surveys, usually coinciding with hurricane events that hit the Outer Banks. Between 2012 and 2020, 46 CLARIS surveys were completed which include at least a portion of the 6.5 km study site. The only beach nourishment that has occurred within this study time period and within the area of interest was in Summer 2017. For the purposes of this work, we consider the pre-nourishment time period to be from 6 November 2012 to 23 February 2017. It is of note that this initial survey for which detailed 3D morphology data from CLARIS along the whole study site is available is timed shortly after Hurricane Sandy, which made landfall along the US East Coast in October 2012 and which caused considerable beach and dune impacts along the Outer Banks (Brodie, Conery, et al., 2019; Sopkin et al., 2014). Within Duck, these impacts included vertical lowering of the beach face by over 1 m and significant scarping and erosion of the dune face ~ 8–12 m landward relative to the pre-storm profile that included significant damage to ocean-front homes and infrastructure in certain regions. Unfortunately, pre-Sandy CLARIS data was not available along the entire length of the study site, so the impacts from this storm are not directly considered in this study.

The post-nourishment time period is considered as 21 November 2017–10 September 2020, with the start of this time period occurring shortly after beach fill placement and corresponding to a CLARIS survey that had data for the entire area of interest. Detailed analysis is completed on interannual trends, particularly related to differences in dune dynamics within the pre- and post-nourishment time periods, from these CLARIS data. Additionally, with these high temporal frequency data, we also focus on analysis of dune impacts at the storm time scale for select events and on the seasonality of dune growth to determine when, where, and why dunes are growing.

Multiple major storm events have impacted the beaches and dunes in Duck between 2012 and 2020. A collection of pre-/post-storm CLARIS surveys where data for the Duck study area were collected are investigated further. Hurricane Jose passed offshore of the Outer Banks in September 2017, immediately following the beach nourishment. Significant wave heights (H_s) reached up to 4.2 m on 19 September 2017 and had peak wave periods (T_p) between ~11 and 13 s for the duration of the event (Table 2 and Figure 2). For a β_{beach} of 0.1 m/m, it estimated that the maximum TWL reached up to 4.4 m and exceeded the 3 m contour level over 4 high tides for a total duration of 24 hr. Based on the spatially variable pre-storm beach slopes, 94% of locations in the alongshore were expected to have TWLs that resulted in collisional impacts during Hurricane Jose. These high TWLs were caused in part by non-tidal residuals (NTR), calculated as the difference between the astronomical predicted tide and measured SWL, of up 0.85 m that coincided also with a spring tide. CLARIS data was collected on 18 September 2017 before the storm and 22 September 2017 immediately following the storm.

Two years later, Hurricane Dorian made landfall in the southern Outer Banks on Hatteras Island (~100 km south of Duck) on 6 September 2019. This is a recent storm of record for the area with peak H_s of 4.4 m at the 17 m wave gauge and over 6 m as measured at other FRF wave gauges, although the storm passed by the Duck region within a matter of hours. The highest H_s did not coincide with the maximum SWL (that included an NTR of up to 1.19 m), resulting in a maximum estimated TWL of only 3.7 m. There were 7 total hours during this event where swash may have been in the collision regime based on the empirically estimated TWLs using a beach slope of

0.1 m/m. Overall, 97% of the Duck dunes were expected to be in the collision regime at some point during Hurricane Dorian based on the spatially variable pre-storm β_{beach}. CLARIS surveys were collected on 4 September 2019 and 10 September 2019 to characterize the impacts of Hurricane Dorian.

Whereas, hurricanes traveling from the Gulf of Mexico or South Atlantic often pass by the Outer Banks relatively quickly, there can be far-field wave events and other storm systems that can result in sustained higher than normal wave energy over multiple tidal cycles across the U.S. East Coast. For example, Hurricane Teddy never made landfall in the continental U.S., but did slowly cross the Atlantic and resulted in long-period waves that reached the beaches of the Outer Banks. The event had maximum H_s, T_p, NTR, and TWLs of 4.0 m, 20 s, 0.54, and 4.5 m, respectively. There were 66 hr over about 10 high tides, coinciding with spring tide conditions, during which the TWL may have reached the 3 m contour and 10 hr where the predicted TWL exceeded 4 m assuming a beach slope of 0.1 m/m. The entire stretch of the study site was predicted to be in the collision regime at some point during Hurricane Teddy. CLARIS data was collected on 10 September 2020 and 25 September 2020 to characterize impacts primarily related to Hurricane Teddy.

Nor'Easters also commonly impact the region. CLARIS data was collected on 14 November 2019 and 19 November 2019, during which interval H_s reached up to 4.8 m. Positive NTRs, up to 0.79 m, occurred coincident with the elevated wave energy. Empirically estimated TWLs suggested that the dune toe was impacted 45 total hours during this period, with maximum TWLs of 4.4 m (assuming a beach slope of 0.1 m/m) contributing to these collision impacts. During this Nor'Easter it is estimated that 100% of the dunes in the study site experienced dune collision during this event based on the pre-storm β_{beach} measurements from CLARIS.

There were other local and far-field events that resulted in predicted collisional dune impacts in this period from 2012 to 2020, as shown by the red dots in Figure 2i. However, as closely spaced pre-/post-storm morphology data is not available for most of these other impactful events.

2.4. Morphology Data Processing

For this study, the raw lidar returns data from CLARIS were filtered to determine the bare-earth bed elevation using standard Riegl terrain filters within the RiScan Pro software. Data was rotated into a local coordinate system that is oriented according to a regional shoreline angle (69.97° represents shore-normal) where $y = 0$ m falls within the FRF property. The filtered data is gridded onto a 0.25 m grid in both the cross-shore and longshore directions for the entire 6.5 km stretch of coast to generate a regional digital elevation model (DEM) for each data collection (e.g., Figure 3). A secondary filter is further applied on each gridded DEM to remove cells with sparse data points near the dune crest where vegetation can limit accurate detection of the bed (e.g., Conery, Cohn, et al., 2020). Errant returns are additionally removed from the gridded surface using a cross-shore Gaussian smoother.

These processing approaches result in high detail elevation grids, although there are still potential errors associated with the definition of the bed. Potential source errors from individual surveys include imperfect positioning information (e.g., RTK GPS, and IMU uncertainty) or vegetation sources, which can typically be treated as having randomly distributed uncertainty for individual points. Therefore, while no rigorous error propagation has been completed here due to the scale of the data, these errors are further minimized within this analysis by focusing on spatially averaged products and ~interannual trends (to be described). These potential sources of error are nonetheless important to consider when interpreting these topographic data and resultant outputs.

Useable data usually extends ~1 m or less below the dune crest for CLARIS scans following the filtering steps. Dune volumes (V_{dune}) are calculated from the total cross-sectional area between 3 and 8 m elevation. This upper limit encapsulates the region approximately up to the dune crest. In some locations, the dune crest height does not exceed 8 m, in which case volumes would represent the volume up to the highest point of useable CLARIS data. For data cells close to the dune crest where data was not available in a particular survey, a no-change condition from the previous survey is assumed for that cell. The 3 m elevation is chosen based on the approximate average dune toe elevation calculated from all of the available data using pybeach (Beuzen, 2019). This implementation of pybeach utilizes a pre-compiled machine learning algorithm that uses Random Forest classification and which was pre-trained on profiles and manually selected dune toe elevations and locations from similar, sandy coastal dune systems. The change in dune volume (ΔV_{dune}) above this 3 m dune toe represents the volumetric change in the total measured dune volume over a fixed time interval, such as within storm events. The rate of change in dune

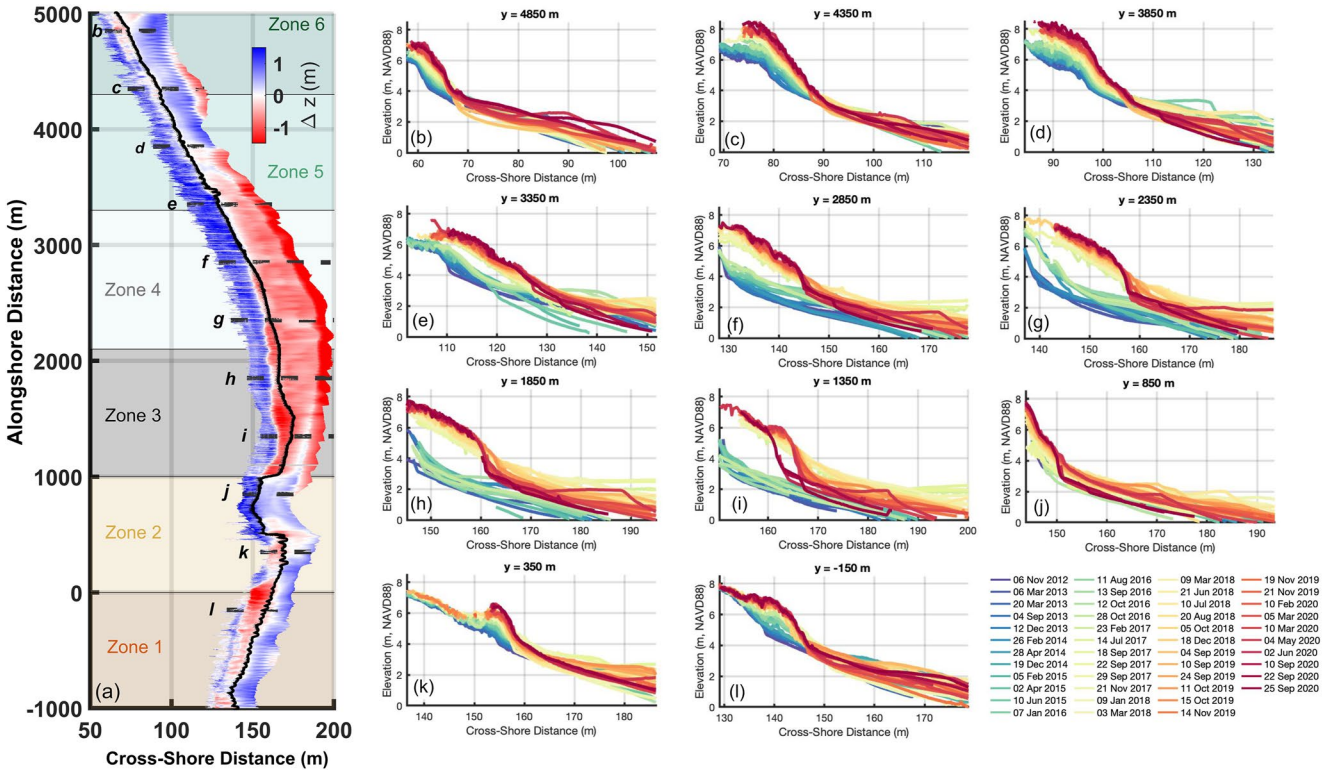

Figure 3. A 3D gridded representation of topographic change in the post-nourishment time period (21 November 2017 to 10 September 2020) where the vertical elevation represents the 21 November 2017 topography and the solid black line shows the location of the 3 m contour. The extents of each of the six zones are shown by the colored polygons. Dashed black lines show the locations of transects shown in panels (b–l). These example cross-shore profiles show topographic change from selection locations throughout the study site for the entire period of record from 6 November 2012 (blue) to 25 September 2020 (red). The nourishment, which included the construction or expansion of dunes at the profiles shown in panels (e–i), occurred in summer 2017.

volume (dV_{dune}/dt) is also reported based on end-point values of V_{dune} in order to normalize the data and allow for intercomparison between different zones and time periods.

Although CLARIS is usually driven at low tide and includes data at and below MHW for the majority of scans, during stormy periods higher TWLs limit the dry, driveable beach. Thus the 1 m elevation is chosen as the lower limit for calculating beach parameters based on broader availability of CLARIS data over time and space. Beach volumes (V_{beach}) are measured as the total volume between 1 and 3 m elevations within each cross-shore transect of data within the DEM region for each of the 44 dates. For any time period or location where CLARIS did not successfully collect data down to 1 m, the local V_{beach} was not calculated. Similarly to V_{dune}, V_{beach} is calculated from the 0.25×0.25 m gridded data and, consistent with typical conventions, are reported as volume changes per meter extent of shoreline in the alongshore. Similarly to the dune region, ΔV_{beach} and dV_{beach}/dt are also calculated from these data. The cross-shore distance of the seaward-most 1 m (x_{1m}) and 3 m (x_{3m}) bed locations was recorded to determine β_{beach}. This end-point slope neglects intermediate details of the beach profile, such as berms and other curvature, although is common approach used to define general geometric attributes of the beach. Because the exact location of dune crest is poorly defined with the CLARIS data due to line of sight limitations and given that the crest of the dune is not above 8 m at all sites (e.g., Figures 3b–3l), a dune slope is not calculated.

All relevant volumetric and geometric metrics that were computed for the beach and the dune for each 0.25 m in the alongshore for each of the 46 surveys are then averaged in 5 m alongshore bins for subsequent analysis. The binning step serves to reduce highly local (e.g., single cross-shore transect) variability in measured morphological changes, including around sand fences and dune walkway cut-throughs, to allow for improved understanding of the causation of observed morphologic changes. For the purpose of further quantifying general regional behavior and implications of differing management styles on dune evolution, the data is further subset and averaged into six alongshore zones that are each approximately 1 km in length (Table 1) for portions of the analysis.

To isolate the seasonal aeolian contribution to dune growth, the gridded morphostratigraphic approach of Cohn et al. (2018) was utilized. The timing and vertical locations of net aeolian deposition was recorded independently for each cross-shore transect in the alongshore from the 0.25 m DEM. Using this method erosional periods are ignored in order to isolate dune growth mechanisms, which are primarily driven by wind-driven sediment fluxes. From the cross-shore transects, volume changes are calculated per 0.01 m vertical elevation within the dune using this morphostratigraphic method and summed to determine the location and timing of net accretional inputs to the dune ($\Delta V_{dune,accretion}$), with the corresponding annual rates of dune growth expressed as $dV_{dune,accretion}/dt$. The method is calculated on all of the available data, except that net changes associated with the dune construction corresponding to bed elevation changes between surveys from 14 July 2017 and 18 September 2017 were removed to isolate only natural dune growth processes. For the purposes of the seasonal investigation, Fall is considered the period from September to November, winter is December to February, Spring is March to May, and Summer is June to August.

3. Field Observations

3.1. Interannual Timescale: 2012–2020

3.1.1. Beach Evolution

Representative cross-shore transect profiles from the dune crest to the water line for each of the 46 CLARIS surveys are shown in Figure 3 across the length of the study site. The beach topography is temporally and spatially variable, with a vertical envelope of variability of up to ~2 m on the beach in some locations (Figure 3). The zone-averaged ΔV_{beach} within each zone (Figure 4c) typically varied by only ±10 m^3/m between subsequent surveys in the pre-nourishment time period. However, there is alongshore variability in ΔV_{beach} within this time period as shown in Figure 5g. For example, ΔV_{beach} within Zone 4 ranged from 3 to 30 m^3/m of growth within the pre-nourishment time period, as extracted from the 5 m binned alongshore data.

The construction of the beach nourishment resulted in a large, rapid increase in V_{beach} (>50 m^3/m) within Zones 3 and 4 (Figure 4c). Following construction, the beach in this nourishment region steadily lost volume at ~ monthly scales up to the end of 2020. Despite these sediment losses, V_{beach} at the end of the post-nourishment period still exceeded the average pre-nourishment V_{beach} in Zones 3 and 4—indicating that some of the nourished sands were retained within the subaerial portion of the system ~3 yr after nourishment. Similar trends were observed with β_{beach} within the nourishment region (Figure 4e). Mild beach slopes (β_{beach} < 0.05 m/m) were measured immediately post-nourishment, with slopes gradually steepening to similar β_{beach} from before beach nourishment (β_{beach} ~ 0.1 m/m).

As sediment was lost from the nourishment zone immediately following the nourishment construction, average beach volumes within Zones 1, 2, and 5 increased throughout 2017 and 2018 (Figure 4c). Beach slopes shallowed in all zones except zone 2 from the start to end of 2017 (Figures 4e and 4f). Zones 1, 2, and 5 all had the highest recorded V_{beach} in the year following nourishment, relative to the rest of the record. However, these volume gains were relatively short-lived, with beach volumes returning to the pre-nourishment beach volume by the end of 2019 (Figures 4c and 4d) in Zones 1, 2, and 5. There were not consistent increases in V_{beach} in Zone 6 in this post-nourishment time period.

3.1.2. Dune Evolution

On average, the coastal foredunes in the region have been both vertically aggrading and prograding (Figure 3) during the study time period. Over the 2012–2017, pre-nourishment time period, the dunes accreted ($\Delta V_{dune} > 0$) along 91% of the study area overall (Figure 5a). In the years after the nourishment, the portion of accreting dunes decreased to 83% of the study area. Zone 2 had both the largest recorded negative ΔV_{dune} and lowest proportion of accretional area (68%) of anywhere in the study site during the pre-nourishment time period. Over this time period, the dunes in Zone 2 lost an average of 1.2 m^3/m and was the only zone with a negative average ΔV_{dune}. This erosional trend reversed in the post-nourishment time period within Zone 2. In the period from late 2017 to 2020, there was an average 8.1 m^3/m net dune growth, with 83% of the Zone 2 dunes being accretional over this time period.

The proportion of dunes that were erosionally increased in Zone 1 between before (90% accretional, 10% erosional) and after (56% accretional, 44% erosional) the nourishment (Figures 5a and 5b). Similarly, in Zone 3

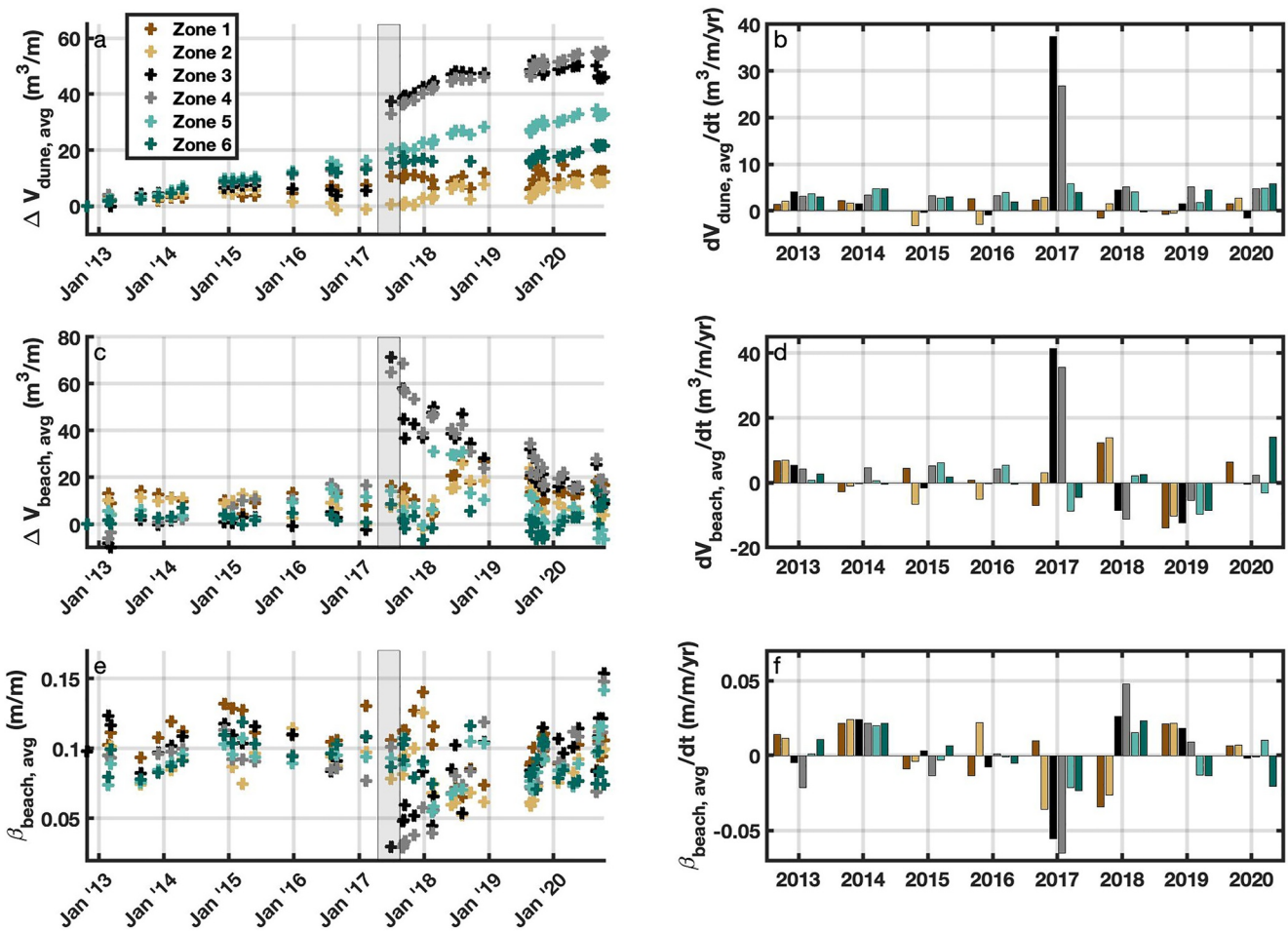

Figure 4. Time series of zone-averaged dune volume change (panel (a)), beach volume change (panel (c)), and beach slope (panel (e)) throughout the period of interest. The gray shaded region represents the nourishment time period in Zones 3 and 4. Net annual volumetric (and beach slope) changes are shown in panels (b and d) (panel (f)).

the proportion of erosional area increased from before (86% accretional, 14% erosional) to after (68% accretional, 32% erosional) nourishment. In Zones 4, 5, and 6 the dunes were accretional in >95% of region both before and after nourishment. Annually normalized beach and dune growth rates are shown in Figures 6a–6f. The zone-averaged annual dV_{dune}/dt only decreased in Zones 1 and 6 in the post-nourishment time period. The change in dV_{dune}/dt, either positive or negative, only exceeded 3 m^3/m/yr in Zone 2. dV_{beach}/dt was similar (±2 m^3/m/yr) before and after nourishment in Zones 1, 2, 5, and 6. Annualized average beach volume losses were much higher in the post-nourishment time period in Zones 3 and 4 associated with beach fill re-equilibration.

The isolation of net accretional conditions using the morphostratigraphic approach indicates that there have been alongshore variable accretion patterns across the foredune face throughout the study region. The annual dune accretion rate was 2.9 m^3/m/yr on average within Duck (Table 3) when removing volume changes associated from anthropogenic input of sediment by ignoring net changes to V_{dune} during the construction period. The highest annual average $dV_{dune,accretion}/dt$ occurred in Zones 4 and 5 and lowest rates in Zones 1 and 2. The distribution of where wind-blown sediments were deposited in the dune also varied spatially within the study site (Figure 7). The morphostratigraphic analysis indicates that a larger proportion of accreted sediments within regions that are actively managed are deposited at high dune elevations (>6 m; Figure 7a) relative to their unmanaged counterparts. Overall 40.2% of observed dune accretion was noted above 6 m in the partially managed dune sections (Zones 1, 5, and 6), 34.6% in the constructed dune region (Zones 3 and 4), and only 23.0% in the unmanaged zone (Zone 2). Conversely, 37.7%, 38.7%, a 48.0% of total sediment gains are located below 5 m for the same zones, respectively.

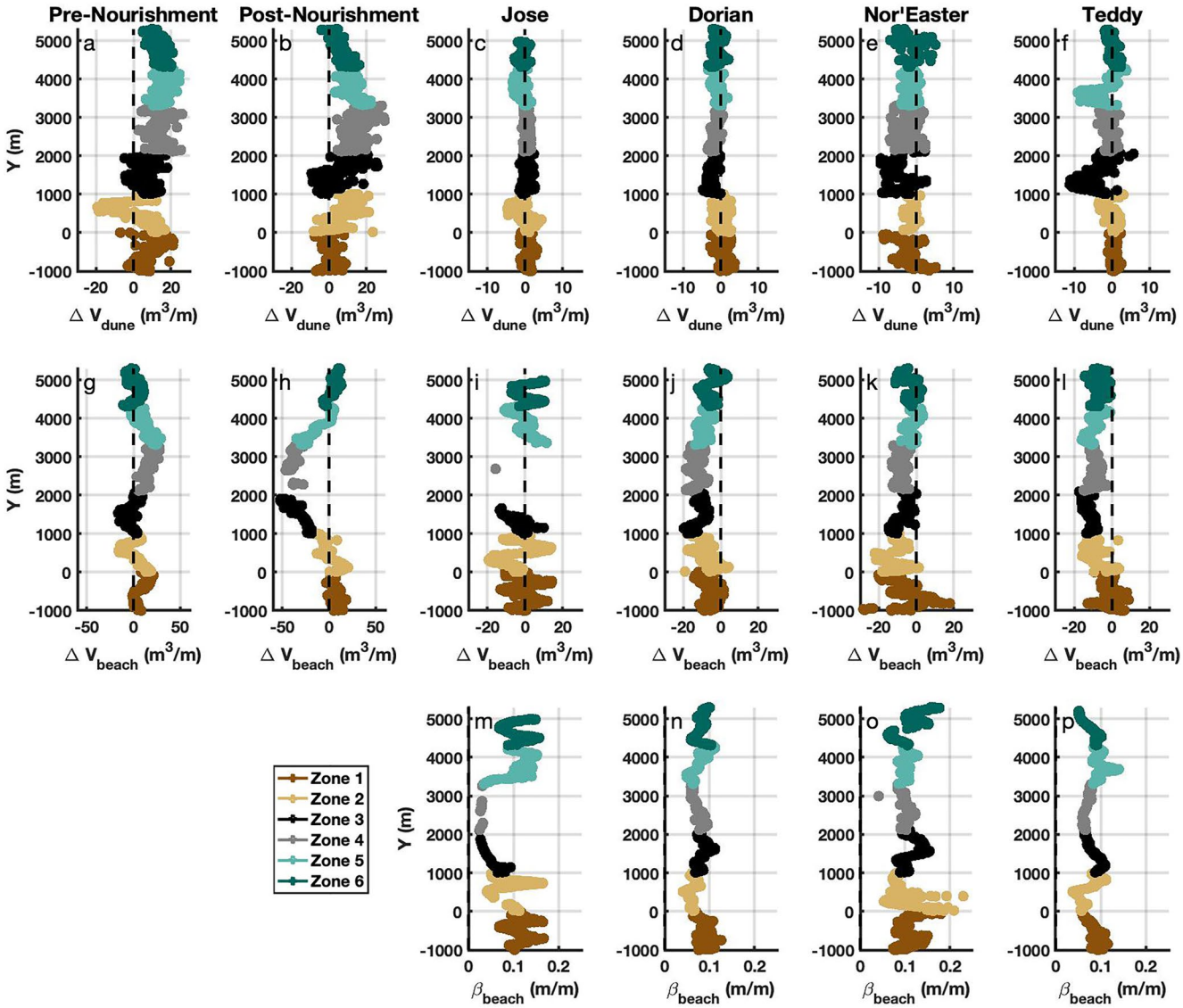

Figure 5. Dune (panel (a–f)) and beach (panels (g–l)) volume changes from the pre-/post-nourishment time periods and for specific storm events. Additionally, pre-storm beach slopes are shown in panels (m–p).

3.1.3. Beach and Dune Interaction

The CLARIS data shows that dune growth rates have the potential to be higher on lower-sloping (more dissipative) beaches sections (Figure 8), although there is considerable scatter in these trends. For example, Zone 4 generally had among the lowest β_{beach} (avg β_{beach} = 0.086 m/m) and the highest average dune accretion rates ($dV_{dune,accretion}/dt$ = 3.2 m^3/m). While similar average β_{beach} existed across the entire study period in Zone 2 as in Zone 4, Zone 2 had much lower net dune accretion rates ($dV_{dune,accretion}/dt$ = 1.6 m^3/m). Conversely, Zone 2 had similar lower net dune accretion rates to Zone 1, although Zone 1 had much higher β_{beach} (avg β_{beach} = 0.107 m/m). The data points in Figure 8 show tight clustering within each zone.

When considering collisional impacts according to the framework of Sallenger (2000) and for calculating dune volume changes, a definition of the dune toe is necessary. The 3 m elevation contour used throughout this work represents the regional average from the entire data set derived using Beuzen (2019), however, there is considerable spatio-temporal variability in this metric. Figure 9a shows that the time-averaged predicted dune toe elevation using pybeach in Zone 3 is the lowest among all regions at 2.65 m elevation. The highest zone-averaged dune toes are located in Zones 1 and 5 with 3.06 and 3.10 m, respectively. When applying the temporally averaged β_{beach} at

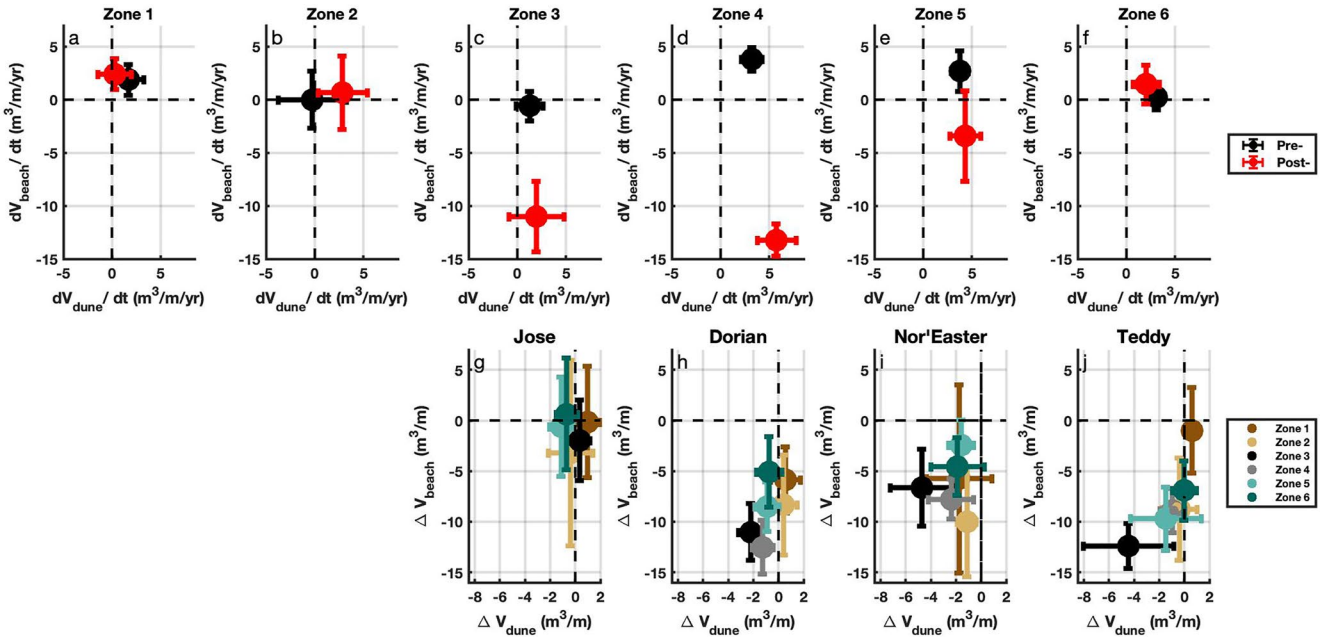

Figure 6. End-point annual beach and dune volume change rates for the pre-nourishment (black) and post-nourishment (red) time periods (panels (a–f)) and end-point beach and dune volume changes rates for each example storm event (panels (g–j)) for each zone. Dots represent the regional average value, with bars representing values ±1 standard deviation.

each 5 m alongshore location with the composite wave runup predictions for the full environmental time series (as shown in Figure 2), this local variability in the dune toe elevation results in predicted dune collision occurring on average 1.3% of the time and up to 2.0% of the time throughout the year at the most vulnerable locations (lowest dune toe and steepest β_{beach}) within Zone 3 (Figure 9b). Conversely, collision was estimated at only 0.2% of the time at the least vulnerable portion of Zone 5. On average, Zones 1, 2, 4, 5, and 6 had zone-averaged collision frequencies of 0.9%, 0.7%, 0.9%, 0.5%, and 0.7% of the time, respectively. Within some individual zones (e.g., Zones 1, 2, and 6), there is a weak ($R^2 \leq 0.4$) but statistically significant relationship between the estimated time in the collision regime and the net ΔV_{dune}. The time in the collision regime explains more variance in ΔV_{dune} than the average dune toe elevation alone (not shown) for the majority of the zones, indicating that the duration of dune collision is likely an important factor to consider in regionally variable dune responses across timescales.

Table 3
Average Volumetric Dune Accretion Rate per Season and Year, in m³/m/yr, for Each Zone

Region	Total	Fall	Winter	Spring	Summer
Zone 1	1.7	0.8	0.3	0.3	0.2
Zone 2	2.1	0.8	0.5	0.3	0.2
Zone 3	3.0	1.4	0.5	0.4	0.3
Zone 4	4.3	1.4	1.1	0.8	0.6
Zone 5	3.9	1.2	1.2	0.8	0.5
Zone 6	2.5	0.8	0.8	0.6	0.2
All	2.9	1.0	0.7	0.5	0.3

3.2. Event to Seasonal Timescale

3.2.1. Seasonal Patterns in Dune Accretion

Trends in beach and dune evolution were highly variable in time, in part dependent on seasonality in environmental forcings. Although dunes can grow any time of the year when wind speeds exceed the threshold velocity, the morphostratigraphic analysis shows that dune volume gains were not equally distributed throughout the year (Figure 7). The largest rates of accretion occurred in Fall within all zones (Table 3), constituting between 31% and 47% (depending on the zone) to the total annual dune growth in this season. Despite Spring including some of the most energetic wind speeds (Figure 2l), there was comparatively lower $dV_{dune,accretion}/dt$ in this season for all zones. Summer was the period with the lowest average volumetric change to the dunes.

Vertical aeolian deposition patterns also do vary seasonally, with the unmanaged coastal extent especially differing in Summer and Fall relative to the other managed coastal extents (Figures 7b–7e). Specifically, there is more

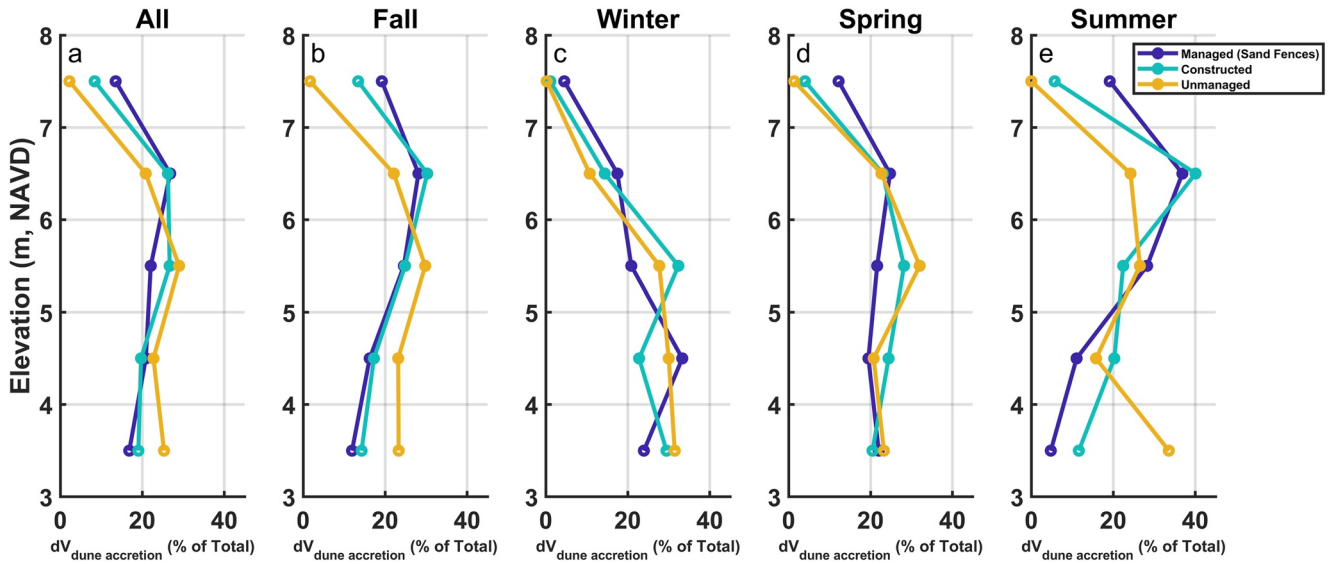

Figure 7. Normalized patterns in the vertical distribution of accreted sediments for each set of dune management types, including those that are partially managed (Zones 1, 5, and 6), recently constructed and actively managed (Zones 3 and 4), and unmanaged (Zone 2), using the morphostratigraphic approach for (a) all months, (b), Fall, (c) Winter, (d) Spring, and (e) Summer.

relative sediment gain to the lowest elevation dune segments (<4 m) on unmanaged dune sections, relative to their constructed or managed counterparts in these seasons.

3.2.2. Storm-Driven Dune Response

3.2.2.1. Hurricane Jose

Shortly following nourishment construction, Hurricane Jose impacted the Outer Banks. This event led to alongshore variable ΔV_{beach}, with zones of both beach growth and beach erosion observed during this event (Figure 5i). On average there was a mean ΔV_{beach} of -1.3 m^3/m during the storm across all zones, although some data gaps within the nourishment zone existed due to incomplete coverage to the 1 m contour. Zone 2 had the highest volume losses to the beach compartment during Hurricane Jose. However, while there was 3.2 m^3/m lost on average from the beach during Jose in Zone 2 (Figure 6g), the northern-most part of this zone immediately adjacent to the nourishment gained up to 14 m^3/m during the storm (Figure 5i).

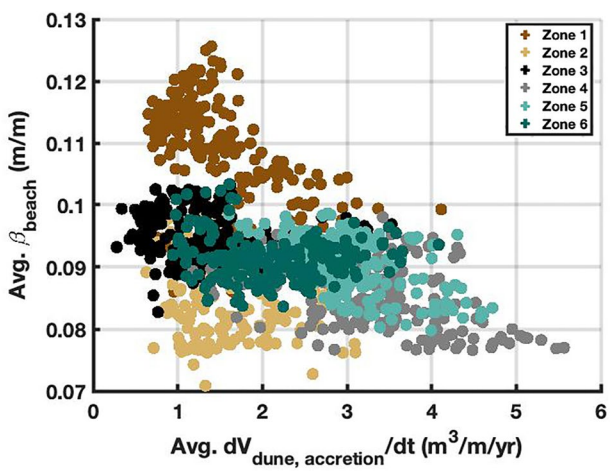

Figure 8. Net annual accretional volume gains from plotted against average β_{beach}.

There was similarly wide variability in dune impacts during the storm (Figure 5c). The mean zone-averaged ΔV_{dune} during Hurricane Jose was ~0 m^3/m. Zones 2, 5, and 6 all had mean negative ΔV_{dune} throughout the storm. Both Zones 2 and 6 had locations where dune erosion was -5 m^3/m or greater. In Zones 5 and 6, these volume losses were related to erosion near the base of the dune (Figures 10q and 10u), whereas in Zone 2 this is attributed primarily to net erosion of the dune face between 4 and 7 m (Figure 10e). There were positive mean ΔV_{dune} in Zones 1, 3, and 4. In Zone 3, the nourished section that had the most dune erosion over the post-nourishment period (Figure 5b), none of the variance (R^2) in ΔV_{dune} was explained by β_{beach} during Hurricane Jose (Figure 11a).

3.2.2.2. Hurricane Dorian

Beach volume losses were widespread during Hurricane Dorian, with 97% of the study area having a negative ΔV_{beach} and 38% of the region having more than -10 m^3/m of ΔV_{beach}. The average volume of sediment lost from V_{beach} was 8.7 m^3/m across all zones. Dune erosion was similarly geographically widespread (71% of the region with $\Delta V_{dune} < 0$), although with less magnitude than ΔV_{beach}. The average ΔV_{dune} was -0.8 m^3/m. Up to 4.7 m^3/m of

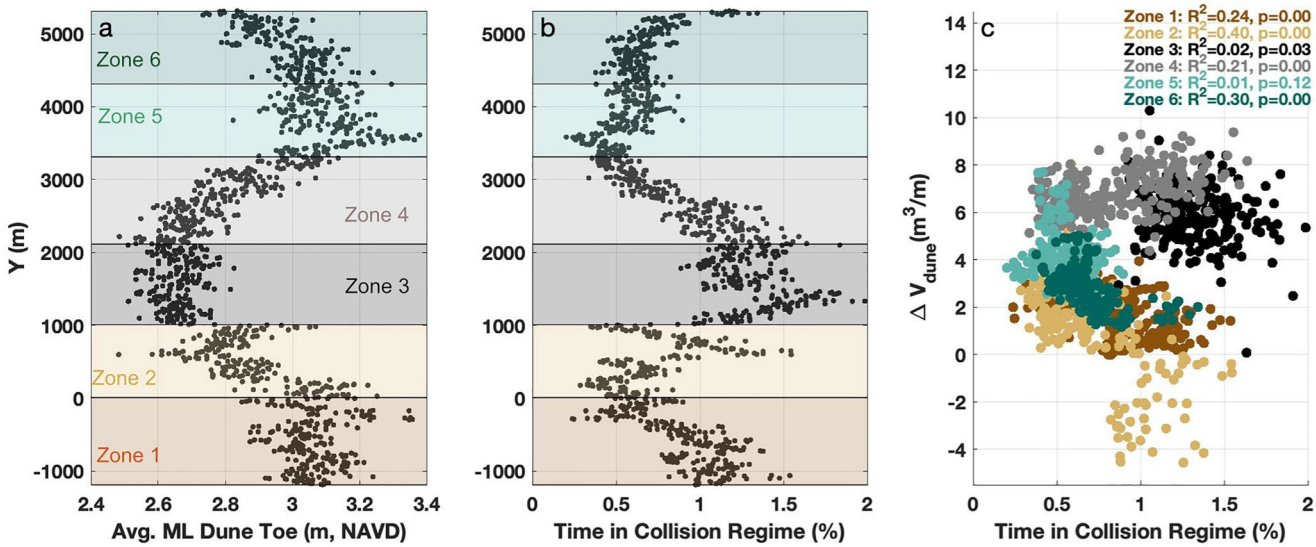

Figure 9. (a) Alongshore variable mean dune toe elevation derived from Beuzen (2019) and (b) the frequency of total water levels exceeding the dune toe at each alongshore extent, utilizing the local mean β_{beach} as input. Panel (c) shows the time in the collision regime vs. total dune volume changes across the entire study time period.

sediment was lost from the dune, with this most extreme value located in Zone 3. In Zones 3–6, there was erosion close to the dune toe elevation as measured between the pre- and post-storm CLARIS surveys (Figure 10). Minor (~1 m) vertical dune scarps were noted in Zone 3 s shown in Figure 1e. While this energetic storm did cause dune erosion in many locations with Duck, there were sediment gains to the dunes, on average, in both Zones 1 and 2 during this event (Figure 6h). There were minimal volumetric changes to the dune near the 3 m base of the dune in Zones 1 and 2, although deposition was observed between 4 and 6 m elevation (Figures 10b and 10f). β_{beach} is a statistically significant variable that explains over 40% of the variance in ΔV_{dune} in Zones 4 and 5, although explains 20% or less of the variance in the remaining zones (Figure 11b).

3.2.2.3. Nor'Easter

The Nor'Easter event which impacted the Outer Banks in November 2019 eroded 92% of the beaches within the study domain. An average of 6.2 m^3/m was lost from V_{beach} during this time period. An average of 2.2 m^3/m was also lost from the dune throughout the entire study site between 14 November 2019 and 19 November 2019. 88% of the dunes in this region were erosional, with Zones 3 and 4 having the highest volumetric losses of the dune of any region during this storm (up to −8 m^3/m). Volumetric erosion between 3 and 4 m elevations was noted, on average, within all six zones (Figures 10c, 10g, 10k, 10o, 10s, and 10w). Zone-averaged volume changes at other elevation bins were close to zero within all six zones.

3.2.2.4. Hurricane Teddy

The volumetric beach erosion from the far-field waves of Hurricane Teddy was among the largest of any of the studied storm events, with 95% of the study domain experiencing beach erosion with an average loss of −8.3 m^3/m during the storm. There were more alongshore variable impacts to the dunes associated with the waves from Hurricane Teddy. There was a zone-averaged loss of −0.5 m^3/m from the dunes. In Zones 1 and 6, the dunes on average gained volume during the event (Figure 6j), primarily between 3 and 4 m elevations (Figures 10d and 10x), whereas Zone 3 had the highest volume losses averaging −4.4 m^3/m within that single zone. Field evidence from Zone 2 indicates that TWLs did reach the dune during Hurricane Teddy and contributed to regions of both new dune scarping and zones with wrack deposition within the vegetated portion of the dune (not shown) where no discernible erosion could be observed. Overall, 56% of the dunes in the entire study site were erosional, whereas 44% of the dunes accreted during this time period. Dune erosion within Zones 2–5 were mostly limited to the lower portion of the dune (<5 m). During swells from Teddy, β_{beach} explained 69% of the variance in ΔV_{dune} in Zone 3—suggesting that β_{beach} was important for controlling where dunes were most impacted (Figure 11d).

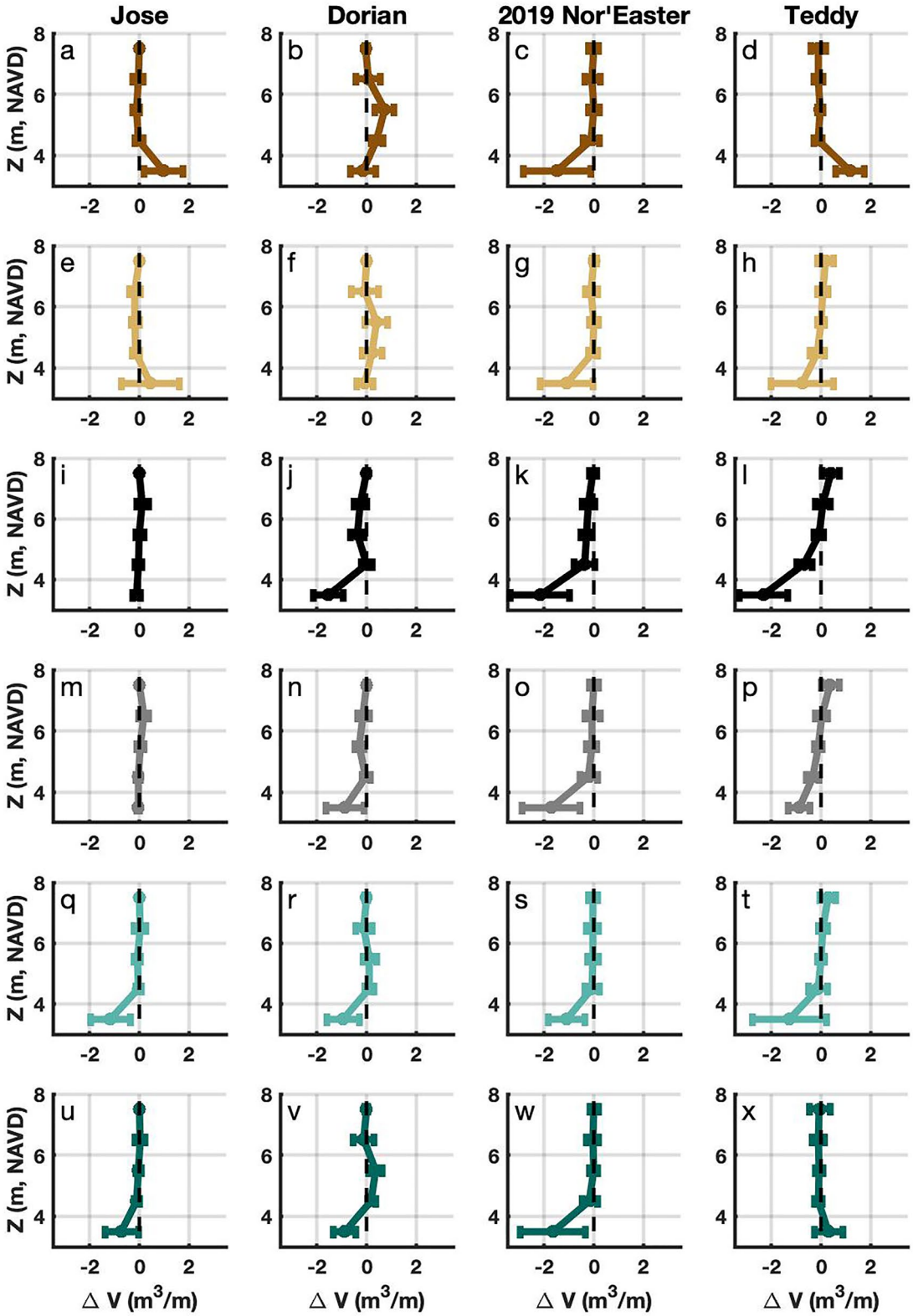

Figure 10. Vertical volumetric changes in 1 m vertical segments for Hurricane Jose (column 1), Hurricane Dorian (column 2), a 2019 Nor'Easter event (column 3), and Hurricane Teddy (column 4) for zones 1 (panels (a–d)), 2 (panels (e–h)), 3 (panels (i–l)), 4 (panels (m–p)), 5 (panels (q–t)), and 6 (panels (u–x)). Dots represent the regional average value for each elevation bin, with bars representing values ±1 standard deviation.

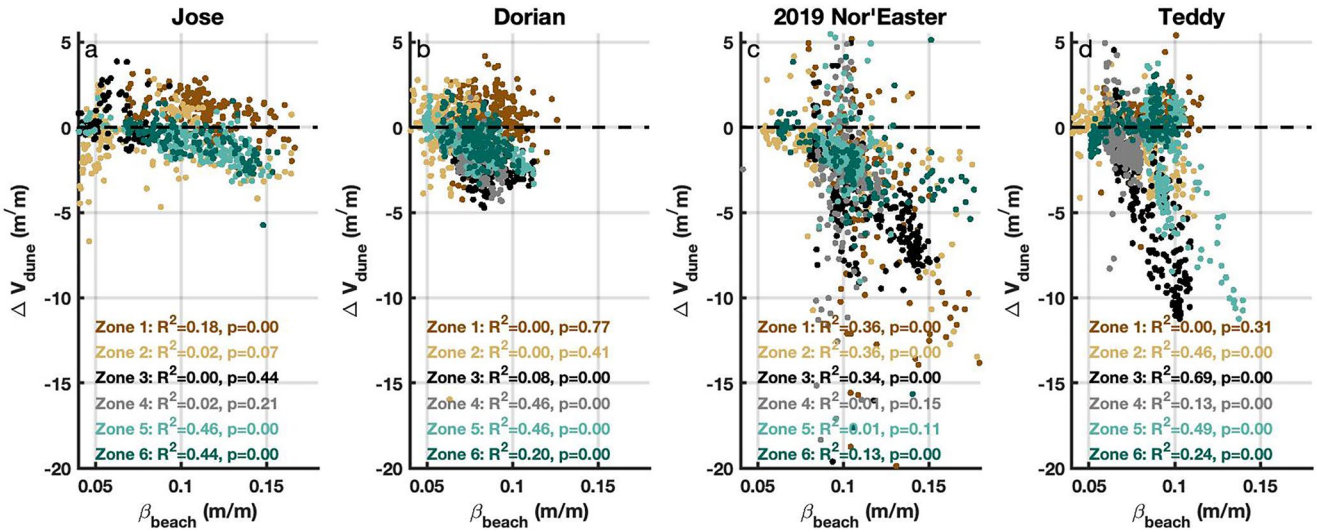

Figure 11. Pre-storm beach slope plotted against volumetric dune erosion for four storm events.

4. Discussion

4.1. Field Insights Into Dune Morphodynamics

4.1.1. Morphologic Controls

Consistent with previous observations of beach-dune interaction (Burroughs & Tebbens, 2008; Cohn et al., 2019; Héquette et al., 2019; Richter et al., 2013), there is some dependency of dune volume losses on pre-storm β_{beach} shown by the CLARIS data (Figure 11) in many circumstances. The relative importance of β_{beach} on ΔV_{dune} varies widely between zones and different storms, with many locations where zero or very low variance in ΔV_{dune} explained by β_{beach}. This observation suggests that while locations with steeper β_{beach} can be more susceptible to wave runup (e.g., Stockdon et al., 2006) and resulting erosion during discrete events, there are likely additional environmental, morphologic, and/or ecological factors at play that influence or control the scale of these potential erosional volumes. For example, the most negative ΔV_{dune} often co-occur with the zones of most negative ΔV_{beach} (Figures 6h and 6j) indicating a possible further coupling between the evolution beach and dune system. Similarly to Garzon et al. (2022), this may suggest that details of the beach morphology beyond β_{beach}, such as the pre-storm backshore volume, are additionally important for explaining spatio-temporal variability in ΔV_{dune}.

Dune growth rates are also often higher on lower-sloping beach sections (Figure 8), in line with the conceptual frameworks of Hesp (1988) and Short and Hesp (1982). Increased wind-blown sediment transport to the dune in these wider beach sections may result from a combination of increased fetch (Delgado-Fernandez, 2010) and smaller median grain size (McFall, 2019) that is easier to mobilize by wind. While there is interannual variability in ΔV_{dune} (Figure 4b), driven by both variability in aeolian accretion and storm-driven erosion, the net growth is fairly linear at interannual scales within each zone (Figure 4a)—consistent with trends noted elsewhere around the world (Cohn et al., 2018; de Vries et al., 2012; Strypsteen et al., 2019). de Vries et al. (2012) previously hypothesized that this linear behavior at interannual to decadal-scale is likely to be related to transport limiting effects, largely due to β_{beach} effects, on aeolian sediment transport. Although the tight clustering of the data in (Figure 8) suggests that additional local morphologic controls, besides just β_{beach}, similarly have equivalent importance on controlling long-term sediment supply to the dune.

The elevation of the dune toe ultimately has important implications for the frequency of collision and the magnitude of potential erosional impacts at the storm timescale (e.g., Figure 9). For example, the comparatively higher duration of TWLs at or above the dune toe elevation may explain why, despite not having the steepest β_{beach} the volume losses during many storm events (Figure 11), is largest in Zone 3 which has among the lowest dune toes. The cause for regional variability in the dune toe remains as of yet unclear. The average pre- and post-nourishment dune toes (not shown) are not substantially different, suggesting some longer-term sedimentological, bathymetric, or other geological control (e.g., Cooper et al., 2018) on the ~5 km alongshore wavelength trend dune toe as

shown in Figure 9a. Since this region with the regionally lowest dune toes coincides with the region that required expensive beach and dune nourishment, better understanding of the causation and implications of this potential geologic control on dune toe variability in the context of dune vulnerability is critically important.

4.2. Environmental Controls

Data from storm timescale indicated that the largest dune erosion events can be associated with multiple-day moderate Nor'Easters, rather than the largest TWL events (Figures 5c–5f). While this is consistent with the important role of wave duration from laboratory studies (e.g., Palmsten & Holman, 2012), field efforts (e.g., Guisado-Pintado & Jackson, 2018), and model results (e.g., Cohn et al., 2019), the literature on this topic is heavily skewed toward documentation for hurricanes and extreme wave events vs. lower peak wave conditions, but longer duration, events such as Nor'Easters. However, it is important to note that in the period of interest there have been no hurricane events that have resulted in overwash or inundation regime impacts, as defined by Sallenger (2000), within this specific region. These more extreme regime classifications would generally be expected to have more catastrophic dune impacts than those in the collision regime. Similarly, pre-/post-morphology data which could be attributed to only a single event was only available for a subset of collisional events, all coinciding with the post-nourishment time period.

Erosion during storms documented by CLARIS was almost always isolated to the regions under 5 m (Figure 10), consistent with the highest predicted TWLs between 2012 and 2020 (Figure 2d). However, the data also show that, simultaneous to erosion of the lower portion of the dune, the dunes have consistently been gaining volume in the ∼decade period of interest in this study. Moreover, some of this wind-driven growth of the upper portion of the dune (>5 m) is shown to occur simultaneously (e.g., during the same event) to wave-driven dune erosion during the investigated storm events (e.g., Figures 10b and 10v). This suggests that aeolian processes may mask some erosional signatures even at the storm timescale in pre and post-storm volume change calculations. This further indicates the importance and complexity of wind-wave-surge sequencing on coastal foredune evolution (e.g., Guisado-Pintado & Jackson, 2018) and the need for frequent surveying to de-couple the relative contributions of wave and wind processes on dune evolution. For example, limited survey data available before 2013 limits a complete quantitative understanding of dune recovery following Hurricane Sandy. Although, the dunes were generally accretive throughout the pre-nourishment time period, in the 5 yr post-Sandy the dunes in the vicinity of Zones 2 and 3 regained less than ∼50% of the original dune face position based on the data that is available. This indicates both the slow timescale of dune recovery relative to storm-driven erosion that is likely further slowed by the multitude of collisional events that happen per year in the Outer Banks.

Interestingly, the largest dune accretion events occur in the Fall months within most zones (Figure 7 and Table 2), coinciding with the period of highest TWL conditions but not necessarily the highest average wind conditions (Figure 2l). Since wind-blown sediment fluxes scale with wind speed (Bagnold, 1937), time-averaged wind speeds are less relevant for predicting wind-blown fluxes relative to the maximum conditions that have some landward-directed component. Both hurricanes and Nor'Easters, which can have high sustained wind speeds, are common during this Fall period. Additionally, the average wind direction for speeds exceeding 8 m/s (representative of storm conditions) is strongly from the north with an onshore, cross-shore component during both September and October (Figure 2n) that promotes sediment flux from the beach to the dune. Conversely, the Spring, which has highest mean wind velocities, has no hurricane events and instead has winds that are more typically from the south and with a mean offshore directed component.

4.3. Anthropogenic Controls

4.3.1. Vertical Distributions of Deposited Sediments

All of the sites saw more volumetric sediment gains at elevations below 6 m than above, although more sediment was deposited at these higher elevations (>6 m) in the managed coastal sections relative to the unmanaged coastal stretch. Nearly 50% of net accreted sediments were observed below 5 m in Zone 2 indicating that there is preferential deposition lower on the dune in this natural region. The cause for these depositional patterns is likely in part related to the location of vegetation and sand fencing which are crucial for producing wind-blown sediment transport gradients. The dune nourishment region initially included regular spacing of sprigs *Ammophila breviligulata*, with additional *Uniola paniculata* planted near the dune crest (CPE, 2017), with similar vegetation present

in the other partially managed coastal sections as well. Conversely, there is a wider range of species present at the unmanaged FRF site including *Panicum amarum*, *Spartina patens*, *Solidago sempervirens*, *Erigeron canadensis*, and *Smilax bona-nox* (e.g., Levy, 1976; Walker & Zinnert, 2022). Quadrat surveys of dune grass vegetation on the dune face in portions of the study site, as presented in White (2022), showed that the total living cover was about twice as high in Zone 2 than Zone 3 and that the species richness was higher in Zone 2 than Zone 3. As different species trap sediment in different magnitudes and styles (e.g., Charbonneau et al., 2021), variable species composition on the dune may contribute to these management-style dependent dune face deposition patterns. This behavior, at least within the nourishment site, may also be related to the lack of well established vegetation following sprigging immediately following construction. Limited vegetation density which would allow sediment bypassing more readily than established, more densely spaced plants.

Sand fencing also plays a critical role for causing sediment transport gradients and therefore influences the spatial distribution of deposited sediments across the dune face. Within Zones 3 and 4 in Duck, 10-foot length sand fences were regularly placed (approximately 2–3 m apart in the longshore) at a 45° angle relative to the coastline in multiple rows across the dune face along with dune construction. Sand fences have been placed throughout Zones 1, 5, and 6, although in a less regular arrangement since dunes in those site were not constructed and therefore had variable topography in the alongshore. Zone 2 has never had sand fences installed. Interestingly, if sand fences are partially responsible for the vertical distribution of deposited dune face sediments, allocating sediment toward the upper part of the dune would generally serve to increase the height of the dune as opposed to dune widening as has been observed along other fenced dune regions (e.g., Itzkin et al., 2020). Observations from Duck supports widespread observations that the details of vegetation, sand fencing, and other obstructions on the dune (e.g., Christmas trees) can modify the deposition patterns within the dune and its subsequent shape, and therefore likely have important implications for the future resilience of that dune system to later storm-driven erosion.

4.3.1.1. Drivers of Increased Sediment Flux to Dune

The exact details of how management factors individually alter the accretion and erosion trends is as of yet unclear, although interestingly the only zone that did not have a positive mean dV_{beach}/dt or dV_{dune}/dt (Figure 6) in the pre-nourishment time period (2012–2017) was Zone 2—the only beach section that had no active management. Instead Zone 2 had slightly negative (~ -1 m^3/m/yr) mean ΔV_{dune} and ΔV_{beach}, with large local variability, in this pre-nourishment period. These trends in Zone 2, relative to the observations from adjacent sections of coast, would suggest that natural settings with no beach or dune management are overall more dynamic, perhaps arising in part due to the lack of efforts to stabilize the dune morphology through fencing, grass planting campaigns, the use of Christmas trees, and, in certain circumstances, sand placement that is present in the other regions.

Dunes in the beach nourishment section naturally accreted following the nourishment at rates that exceeded the pre-nourishment time period (Figures 4 and 6). The largest annual increases in ΔV_{dune} in the nourished section (Zones 3 and 4) coincided with the years immediately following sand placement in 2017 (Figures 4a–4b and 6c–6d). This is consistent with observations from a nearby nourishment in 2011 in Nags Head where data suggests that there was higher than normal aeolian activity in the year immediately following beach fill construction (Kaczkowski et al., 2018). Similarly to the explanations for alongshore variability in sediment to the dune (Section 4.1.1), two mechanisms exist that may contribute to post-nourishment rises in aeolian contributions to dune growth. First, there is a grain size dependence on the threshold velocity (u_t) for wind-blown sand—with smaller grains being capable of being transported under lower wind speeds. Repeat beach grab data from the FRF indicate that the average median grain size (D_{50}) for the region is approximately 0.34 mm. Using Bagnold (1937), the u_t for sands of this size are 7.6 m/s (at 20 m elevation, consistent with the height of the FRF anemometer). Winds that include some onshore wind component are expected to be able to mobilize this median grain size 15.4% of the time at Duck for the study time period (e.g., utilizing the environmental time series shown in Figure 2k) and transport some of the sediments toward the dune. Because aeolian transport rates scale non-linearly with increases in wind speed above the threshold velocity—substantial rates of transport associated with very energetic winds would occur less frequently. The Duck beach nourishment included sediment sourced from two borrow sites, one with a D_{50} of 0.28 mm ($u_t = 6.8$ m/s) and one of 0.36 mm ($u_t = 7.8$ m/s) (CPE, 2017). Additionally, it is noted that there is some fraction of shell hash and coarse material also present in the constructed beach/dune system. For the smaller borrow-sourced D_{50}, u_t would be exceeded for winds with an onshore component 19.2% of the time, whereas median sands from the coarser borrow site are only mobilized 14.5% of the time. This introduction of slightly finer sediments into the system can explain both in an increase in the number of

accretional events per year and the net magnitude of volumetric dune growth immediately following nourishment. Zones that were immediately adjacent to the beach nourishment also saw an increase in dune growth rates in the post-nourishment time period.

Beach width can similarly contribute to increased aeolian activity on beach nourishment sites. There is a minimum distance that it takes for sediment to reach a saturated concentration, referred to as a critical fetch length that determines whether unsaturated or saturated transport occurs prior to the dune. This length scale has been shown to vary widely based on site and environmental characteristics, generally being in the range of tens to hundreds of meters (e.g., Bauer & Davidson-Arnott, 2003; Davidson-Arnott et al., 2008; Delgado-Fernandez, 2010). Assuming a critical fetch length of 20 m (50 m) and utilizing the environmental time series in Figure 2, the resultant occurrence of expected saturated transport before the base of the dune (3 m) would be 13.9% (10.1%), 9.8% (3.3%), and 5.0% (1.5%) for the period from 2012 to 2020 for β_{beach} of 0.05, 0.1, 0.15 m/m, respectively. In this example, β_{beach} of 0.05 m/m is representative of the beach conditions shortly after nourishment (Figure 4e), whereas the average regional β_{beach} is about 0.1 m/m. Independent of other variables (e.g., grain size variation), saturated transport to the base of the dune is likely to occur 1.42 and 3.1 times more often on the recently nourished beach section (0.05 m/m) relative to Duck beaches with slopes of 0.1 and 0.15 m/m, respectively, based on these slopes and fetch constraints.

After the initial ~1 yr following the beach fill construction, the data show a reduction in annual ΔV_{dune} in Zone 3 between 2018 and 2019 (Figure 4b). This trend is similar to observations at Nags Head from Kaczkowski et al. (2018) where aeolian fluxes reduced after the first year following nourishment. In Duck, this trend occurred despite there being more sediment on the beach (high V_{beach}) relative to the pre-nourishment period (Figure 4c). While there was more overall sediment within the 1–3 m elevation contours in this timeframe in Zones 3 and 4, there was a gradual loss in ΔV_{beach} and a steeping in β_{beach} following equilibration of the nourishment (Figure 4e). This increase in β_{beach} in the years following nourishment, associated with the landward retreat of the 1 m contour, would serve to (a) decrease fetch lengths under onshore winds and decrease the occurrence of saturated wind-blown transport to the dunes and (b) increase wave runup and therefore increase the occurrence of dune collision/erosion. Simultaneous to sediment losses from Zones 3 and 4 due to the diffusion of the nourishment, the opposite effect happened on beaches adjacent to the nourishment as ΔV_{beach} increased that may have also modified β_{beach} and contributed to increases in ΔV_{dune}.

4.4. Conceptual Model for Managed and Unmanaged Dune Evolution

From the study findings, we propose conceptual diagrams in Figure 12 which synthesize the relationships between environmental forcings and the various morphodynamic feedbacks of the dune and beach in time and space on unmanaged, managed, and down-drift nearby unmanaged coastlines yielded from the field data. While the same physical processes apply independent of whether a system is allowed to naturally evolve or is anthropogenically modified, the time evolution of the system is heavily dependent on management actions (e.g., Itzkin et al., 2020; N. L. Jackson & Nordstrom, 2011). Upon the occurrence of a beach nourishment (Time 3 in Figures 12a–12d) sediment is typically rapidly lost from the beach-berm system. Assuming a beach slope definition from the dune toe to the shoreline, the beach slopes are instantaneously reduced due to this equilibration of the beach fill placement (Figure 12d). Between times 3 and 4 in Figure 12, if large wind events occur (Figure 12b) it would be expected that aeolian transport rates and corresponding net transport to the dune would be larger on a constructed beach system relative to the same environmental forcings applied to a natural area due to these various fetch and sediment supply effects (e.g., Kaczkowski et al., 2018). The data suggest that aeolian activity is enhanced not just at dunes behind the beach nourishment, but also at adjacent stretches of coast. This is likely to happen especially in regions with large rates of longshore subaqueous sediment transport and/or strongly oblique winds, such as is common in the Outer Banks.

Over time the β_{beach}, as measured from the dune toe to the shoreline, within the constructed region may be expected to gradually increases after the initial placement, reflected by equilibration, sediment losses to the nearshore, sediment losses to the dune, and longshore transport gradients. As the β_{beach} increases and the beach width decreases, the magnitude of net dune growth during windy periods decreases (e.g., Kaczkowski et al., 2018) and the frequency of dune collision from waves increases. A wave event (Figure 12a) that caused no erosion to the dune in the constructed zone at Time 5 may be expected to have much more substantial impacts at a later time after the nourishment (Figure 12c). Thus while the net dune growth in a constructed region may be higher

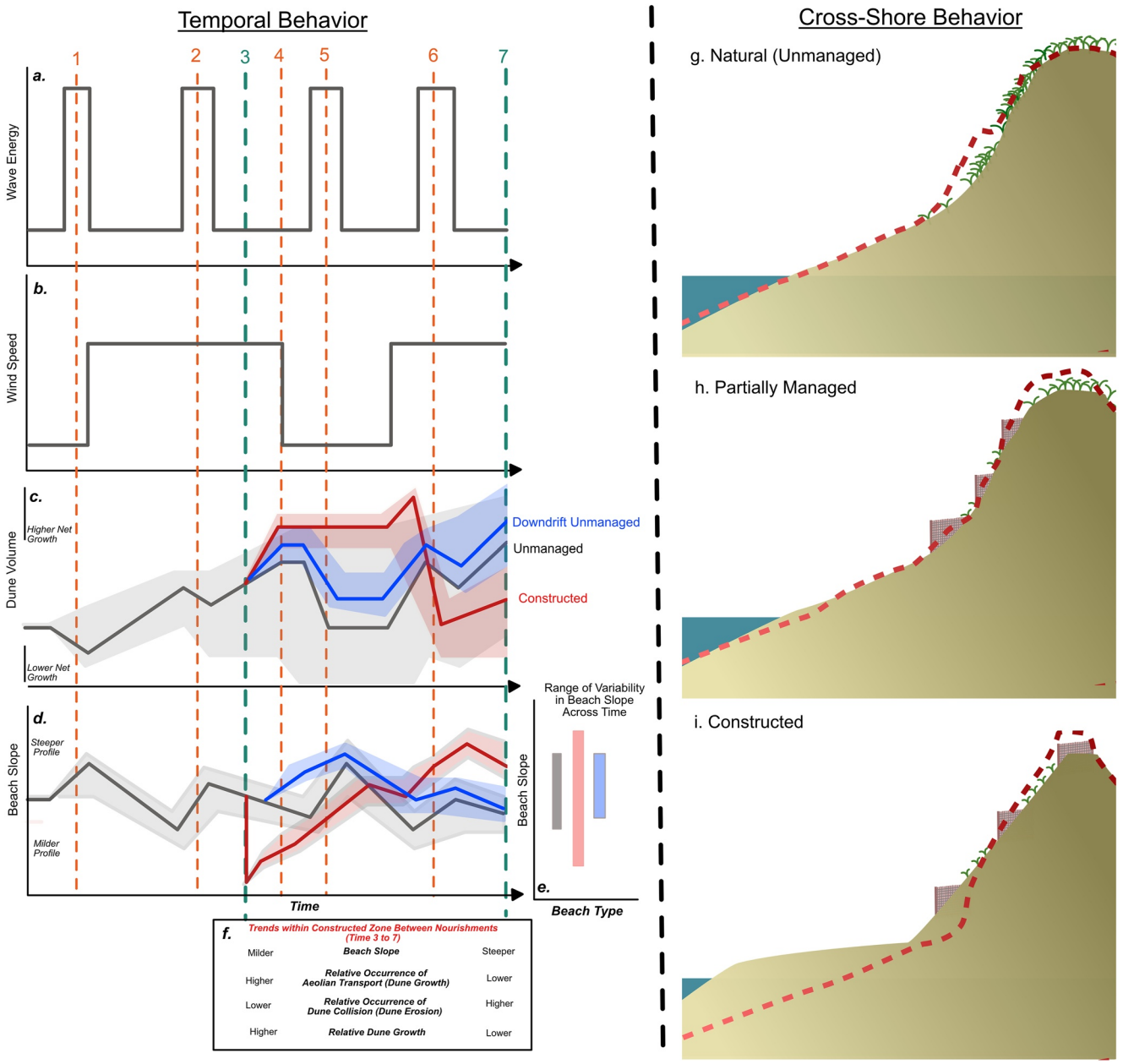

Figure 12. Conceptual schematic of beach and dune changes along natural and constructed dune systems, as well as coastal stretches downdrift of constructed regions. Synthetic time series of waves (panel (a)), winds (panel (b)), dune volumes (panel (c)), and beach slopes (panel (d)) are shown, with the solid lines representing mean responses and shaded regions representing the range (where relevant). Panel (e) shows the total range of possible beach slopes on constructed beaches (red), relative to unmanaged (black) and downdrift (blue) beaches. Various times of references (1–7) are noted by vertical lines on the panels and are described in the text. A general overview of factors that change with time from the start o the beach nourishment from Time 3 to Time 7 are shown in panel (f). A corresponding conceptual schematic of representative cross-shore bed elevation changes relative to the location of vegetation and sand fencing on unmanaged (panel (g)), partially managed (panel (h)), and recently constructed (panel (i)) dunes are also shown. Dotted lines indicate deviations from the initial bed at interannual scale.

between Times 3 and 4, the natural system has the possibility to have relatively higher (or similar) net dune growth between Times 3 and 7 in this simplified framework due to time evolution of the time evolution beach characteristics.

These trends are also influenced by the actual morphology of the dune system. In the case of the constructed dune system, at least as seen in this present study, there is persistent scarping and retreat during storms at the base of the constructed dune (Figure 12i). However, the same constructed dune grew volumetrically throughout the study

period as the bulk of those accumulated sediments were located on the upper portion of the dune face. A trend of overall dune face steepening between the crest and toe is noted along constructed dune systems in this scenario (Figure 12i). Conversely, in this study time periods sediment along natural dune systems was preferentially accumulated lower on the lower dune face relative to the managed regions likely, as schematized in Figures 12g–12i, due to both sediment trapping by vegetation low on the dune face and/or possible contributions of marine deposition within the lower portion of the dune complex (e.g., Cohn et al., 2019) (e.g., Hurricane Teddy).

Consistent with a wide range of other studies (Delgado-Fernandez, 2010; Garzon et al., 2022; Hesp, 1988), the data here collectively indicate that beach morphology has numerous important feedbacks on transport dynamics that contribute to the ability for the dune system to accrete and/or erode. However, other physical, ecological, morphologic, and environmental factors likewise modify these transport dynamics which contributes to the broad potential trajectories of coastal geomorphic evolution (e.g., Time 7 in Figure 12).

5. Conclusions

Coastal foredune evolution is highly three-dimensional resulting from the complex interplay between marine, aeolian, ecological, and anthropogenic processes. On interannual timescales the dunes throughout the study site are growing despite being in the collision regime numerous times per year. Dunes on sections of coast with the lowest β_{beach} generally grow at the highest rates, whereas net volumetric dune growth is lowest on steeper beach sections. This is due in part because these steeper sections are prone to more dune collision during storms due to slope effects on wave runup. Beach nourishment alters the local morphology of the beach which correspondingly alters aeolian transport rates and dune erosion through slope and fetch effects. Increases in ΔV_{dune} were found in the post-nourishment time period behind the beach nourishment zone resulting from reduced frequency from dune collision during storms and enhanced aeolian transport associated with larger beach widths. The distribution of deposited sediments within the dune were also shown to vary between unmanaged and managed sections of coast. Specifically, a larger portion of aeolian deposition occurs at lower elevations (<5 m) on unmanaged beach sections relative to those that have been managed resulting from differences in spatial patterns in vegetation type and density, sand fencing, and/or the shape of the dune between these various stretches of coast. The collective data indicate that beach and dune management alter both the magnitude and form of dune evolution, having important implications for the resilience of dunes to future impacts and the protective services they provide to infrastructure immediately landward of the dune. Specifically, vegetation and sand fencing are both independently important for trapping patterns of wind-blown sands and thus may be used to design more resilient dunes at the storm timescale. However, regionally variable sediment supply effects due to background erosion, grain size controls on beach slope, and anthropogenic additions of sediment predominantly control the magnitude of dune volume growth or erosion and therefore have a relatively more important influence on dictating the long-term trajectory of these features.

Data Availability Statement

All environmental data used in this work can be accessed through the FRF THREDDS server at https://chlthredds.erdc.dren.mil/. Specifically, the 17 m bulk wave statistics data can be found at https://chldata.erdc.dren.mil/thredds/catalog/frf/oceanography/waves/waverider-17m/catalog.html, with data gaps provided at a 26 m buoy as described in the text that can be found at https://chldata.erdc.dren.mil/thredds/catalog/frf/oceanography/waves/waverider-26m/catalog.html. SWL and wind data are also available on the THREDDS server from the oceanography and meteorology folders, respectively. Data can be downloaded as netcdf files from the THREDDS server with no registration required. All CLARIS data collected by ERDC for Duck and the broader Outer Banks for the time period of interest can be found through the Geospatial Research and Data Management System (GRiD) at: https://grid.nga.mil/grid/. Registration is required to access GRiD, but is publicly accessible and instantly available following registration. Data can be searched geographically for the area of interest within the Outer Banks, with data listed by date of survey and listed as being collected by "USACE."

Acknowledgments
This study was funded by ERDC's Flood and Coastal Systems R&D program through the Resilience of Coastal Dunes work unit and by the NOAA's National Centers for Coastal Ocean Science, Competitive Research Program under award NA19NOS4780175 to ERDC. Long-term CLARIS data collection was supported by ERDC's Coastal Field Data Collection program.

References

Armstrong, S. B., & Lazarus, E. D. (2019). Masked shoreline erosion at large spatial scales as a collective effect of beach nourishment. *Earth's Future*, *7*(2), 74–84. https://doi.org/10.1029/2018ef001070

Bagnold, R. A. (1937). The transport of sand by wind. *The Geographical Journal*, *89*(5), 409. https://doi.org/10.2307/1786411

Bauer, B. O., & Davidson-Arnott, R. (2003). A general framework for modeling sediment supply to coastal dunes including wind angle, beach geometry, and fetch effects. *Geomorphology*, *49*(1–2), 89–108. https://doi.org/10.1016/s0169-555x(02)00165-4

Bauer, B. O., Davidson-Arnott, R., Hesp, P. A., Namikas, S., Ollerhead, J., & Walker, I. (2009). Aeolian sediment transport on a beach: Surface moisture, wind fetch, and mean transport. *Geomorphology*, *105*(1–2), 106–116. https://doi.org/10.1016/j.geomorph.2008.02.016

Beuzen, T. (2019). pybeach: A python package for extracting the location of dune toes on beach profile transects. *Journal of Open Source Software*, *4*(44), 1890. https://doi.org/10.21105/joss.01890

Birkemeier, W. A., Dolan, R., & Fisher, N. F. (1984). The evolution of a barrier island: 1930–1938. *Journal of the American Shore and Beach Preservation Association*, *52*(2), 2–12.

Birkemeier, W. A., & Forte, M. F. (2019). *Field research facility: A users guide to the survey lines data set, (Tech. Rep.)*. U.S. Army Engineer Research and Development Center. (ERDC-SR-19-5).

Bridges, T. S., Wagner, P., Burks-Copes, K. A., Bates, M. E., Collier, Z. A., Fischenich, J. C., et al. (2015). *Use of natural and nature-based features (NNBF) for coastal resilience*. U.S. Army Engineer Research and Development Center. (ERDC-SR-15-1).

Brodie, K. L., Bruder, B. L., Slocum, R. K., & Spore, N. J. (2019). Simultaneous mapping of coastal topography and bathymetry from a lightweight multicamera UAS. *IEEE Transactions on Geoscience and Remote Sensing*, *57*(9), 6844–6864. https://doi.org/10.1109/tgrs.2019.2909026

Brodie, K. L., Conery, I., Cohn, N., Spore, N., & Palmsten, M. (2019). Spatial variability of coastal foredune evolution, part A, timescales of months to years. *Journal of Marine Science and Engineering*, *7*(5), 124. https://doi.org/10.3390/jmse7050124

Burroughs, S. M., & Tebbens, S. F. (2008). Dune retreat and shoreline change on the Outer Banks of North Carolina. *Journal of Coastal Research*, *2*, 104–112. https://doi.org/10.2112/05-0583.1

Charbonneau, B. R., Dohner, S. M., Wnek, J. P., Barber, D., Zarnetske, P., & Casper, B. B. (2021). Vegetation effects on coastal foredune initiation: Wind tunnel experiments and field validation for three dune-building plants. *Geomorphology*, *378*, 107594. https://doi.org/10.1016/j.geomorph.2021.107594

Ciarletta, D. J., Shawler, J. L., Tenebruso, C., Hein, C. J., & Lorenzo-Trueba, J. (2019). Reconstructing coastal sediment budgets from beach-and foredune-ridge morphology: A coupled field and modeling approach. *Journal of Geophysical Research: Earth Surface*, *124*(6), 1398–1416. https://doi.org/10.1029/2018jf004908

Cohn, N., Brodie, K. L., Johnson, B., & Palmsten, M. L. (2021). Hotspot dune erosion on an intermediate beach. *Coastal Engineering*, *170*, 103998. https://doi.org/10.1016/j.coastaleng.2021.103998

Cohn, N., Ruggiero, P., de Vries, S., & Kaminsky, G. (2018). New insights on the relative contributions of marine and aeolian processes to coastal foredune growth. *Geophysical Research Letters*, *45*(10), 4965–4973. https://doi.org/10.1029/2018gl077836

Cohn, N., Ruggiero, P., Garcia, G., Anderson, D., Serafin, K., & Biel, R. (2019). Environmental and morphologic controls on wave induced dune response. *Geomorphology*, *329*, 108–128. https://doi.org/10.1016/j.geomorph.2018.12.023

Conery, I., Brodie, K., Spore, N., & Walsh, J. (2020). Terrestrial lidar monitoring of coastal foredune evolution in managed and unmanaged systems. *Earth Surface Processes and Landforms*, *45*(4), 877–892. https://doi.org/10.1002/esp.4780

Conery, I., Cohn, N. T., Spore, N. J., & Brodie, K. L. (2020). *Evaluating collection parameters for mobile lidar surveys in vegetated beach dune settings (Tech. Rep.)*. Vicksburg United States: Engineer Research and Development Center (U.S.). (ERDC/CHL CHETN-II-58). https://doi.org/10.21079/11681/37759

Cooper, J. A. G., Green, A. N., & Loureiro, C. (2018). Geological constraints on mesoscale coastal barrier behavior. *Global and Planetary Change*, *168*, 15–34. https://doi.org/10.1016/j.gloplacha.2018.06.006

Costas, S., de Sousa, L. B., Kombiadou, K., Ferreira, Ó., & Plomaritis, T. A. (2020). Exploring foredune growth capacity in a coarse sandy beach. *Geomorphology*, *371*, 107435. https://doi.org/10.1016/j.geomorph.2020.107435

Cox, N., Dunkin, L. M., & Irish, J. L. (2013). An empirical model for infragravity swash on barred beaches. *Coastal Engineering*, *81*, 44–50. https://doi.org/10.1016/j.coastaleng.2013.06.008

CPE. (2017). Town of Duck shore protection project: Beach maintenance plan. (prepared by Coastal Planning and Engineering of North Carolina, Inc.).

Crowson, R., Birkmeier, W., Klein, H., & Miller, H. (1988). SUPERDUCK nearshore processes experiment: Summary of studies CERC Field Research Facility (Tech. Rep.). (CERC-89-16).

Davidson, S. G., Hesp, P. A., & de Silva, G. M. (2020). Controls on dune scarping. *Progress in Physical Geography: Earth and Environment*, *44*(6), 923–947. https://doi.org/10.1177/0309133320932880

Davidson-Arnott, R., Hesp, P. A., Ollerhead, J., Walker, I., Bauer, B. O., Delgado-Fernandez, I., & Smyth, T. (2018). Sediment budget controls on foredune height: Comparing simulation model results with field data. *Earth Surface Processes and Landforms*, *43*, 1798–1810. https://doi.org/10.1002/esp.4354

Davidson-Arnott, R., Yang, Y., Ollerhead, J., Hesp, P. A., & Walker, I. J. (2008). The effects of surface moisture on aeolian sediment transport threshold and mass flux on a beach. *Earth Surface Processes and Landforms*, *33*(1), 55–74. https://doi.org/10.1002/esp.1527

de Vries, S., Arens, S., de Schipper, M., & Ranasinghe, R. (2014). Aeolian sediment transport on a beach with a varying sediment supply. *Aeolian Research*, *15*, 235–244. https://doi.org/10.1016/j.aeolia.2014.08.001

de Vries, S., Southgate, H., Kanning, W., & Ranasinghe, R. (2012). Dune behavior and aeolian transport on decadal timescales. *Coastal Engineering*, *67*, 41–53. https://doi.org/10.1016/j.coastaleng.2012.04.002

de Vries, S., Verheijen, A., Hoonhout, B., Vos, S., Cohn, N., & Ruggiero, P. (2017). Measured spatial variability of beach erosion due to aeolian processes. In T. Aagaard, R. Deigaard, & D. Fuhrman (Eds.), *Proceedings of the Coastal Dynamics Conference 2017*. Helsignor, Denmark.

de Winter, R., Gongriep, F., & Ruessink, B. (2015). Observations and modeling of alongshore variability in dune erosion at Egmond aan Zee, the Netherlands. *Coastal Engineering*, *99*, 167–175. https://doi.org/10.1016/j.coastaleng.2015.02.005

De Battisti, D., & Griffin, J. N. (2020). Below-ground biomass of plants, with a key contribution of buried shoots, increases foredune resistance to wave swash. *Annals of Botany*, *125*(2), 325–334.

Delgado-Fernandez, I. (2010). A review of the application of the fetch effect to modeling sand supply to coastal foredunes. *Aeolian Research*, *2*(2–3), 61–70. https://doi.org/10.1016/j.aeolia.2010.04.001

Donker, J., Van Maarseveen, M., & Ruessink, G. (2018). Spatio-temporal variations in foredune dynamics determined with mobile laser scanning. *Journal of Marine Science and Engineering*, *6*(4), 126. https://doi.org/10.3390/jmse6040126

Enwright, N. M., Wang, L., Borchert, S. M., Day, R. H., Feher, L. C., & Osland, M. J. (2018). The impact of lidar elevation uncertainty on mapping intertidal habitats on barrier islands. *Remote Sensing*, *10*(1), 5.
Erikson, L. H., Larson, M., & Hanson, H. (2007). Laboratory investigation of beach scarp and dune recession due to notching and subsequent failure. *Marine Geology*, *245*(1–4), 1–19. https://doi.org/10.1016/j.margeo.2007.04.006
Feagin, R. A., Figlus, J., Zinnert, J. C., Sigren, J., Martínez, M. L., Silva, R., et al. (2015). Going with the flow or against the grain? The promise of vegetation for protecting beaches, dunes, and barrier islands from erosion. *Frontiers in Ecology and the Environment*, *13*(4), 203–210. https://doi.org/10.1890/140218
Feagin, R. A., & Williams, A. M. (2008). Sediment spatial patterns in a Hurricane Katrina overwash fan on Dauphin Island, Alabama, USA. *Journal of Coastal Research*, *24*(244), 1063–1070. https://doi.org/10.2112/07-0862.1
Figlus, J., Kobayashi, N., Gralher, C., & Iranzo, V. (2011). Wave overtopping and overwash of dunes. *Journal of Waterway, Port, Coastal, and Ocean Engineering*, *137*(1), 26–33. https://doi.org/10.1061/(asce)ww.1943-5460.0000060
Garzon, J. L., Costas, S., & Ferreira, O. (2022). Biotic and abiotic factors governing dune response to storm events. *Earth Surface Processes and Landforms*, *47*(4), 1013–1031. https://doi.org/10.1002/esp.5300
Grafals-Soto, R., & Nordstrom, K. (2009). Sand fences in the coastal zone: Intended and unintended effects. *Environmental Management*, *44*(3), 420–429. https://doi.org/10.1007/s00267-009-9331-7
Guisado-Pintado, E., & Jackson, D. (2018). Multi-scale variability of storm Ophelia 2017: The importance of synchronized environmental variables in coastal impact. *Science of the Total Environment*, *630*, 287–301. https://doi.org/10.1016/j.scitotenv.2018.02.188
Héquette, A., Ruz, M.-H., Zemmour, A., Marin, D., Cartier, A., & Sipka, V. (2019). Alongshore variability in coastal dune erosion and post-storm recovery, northern coast of France. *Journal of Coastal Research*, *88*(SI), 25–45.
Hesp, P. A. (1981). The formation of shadow dunes. *SEPM Journal of Sedimentary Research*, *51*, 101–112.
Hesp, P. A. (1988). Surfzone, beach, and foredune interactions on the Australian southeast coast. *Journal of Coastal Research*, *3*(3), 15–25.
Hesp, P. A. (1989). A review of biological and geomorphological processes involved in the initiation and development of incipient foredunes. *Proceedings of the Royal Society of Edinburgh—Section B: Biological Sciences*, *96*, 181–201. https://doi.org/10.1017/s0269727000010927
Hesp, P. A., & Smyth, T. A. (2016). Jet flow over foredunes. *Earth Surface Processes and Landforms*, *41*(12), 1727–1735. https://doi.org/10.1002/esp.3945
Hesp, P. A., & Smyth, T. A. (2019). CFD flow dynamics over model scarps and slopes. *Physical Geography*, *42*, 1–24. https://doi.org/10.1080/02723646.2019.1706215
Hodgson, M. E., & Bresnahan, P. (2004). Accuracy of airborne lidar-derived elevation. *Photogrammetric Engineering and Remote Sensing*, *70*(3), 331–339. https://doi.org/10.14358/pers.70.3.331
Inman, D. L., & Dolan, R. (1989). The outer banks of North Carolina: Budget of sediment and inlet dynamics along a migrating barrier system. *Journal of Coastal Research*, 193–237.
Itzkin, M., Moore, L. J., Ruggiero, P., & Hacker, S. D. (2020). The effect of sand fencing on the morphology of natural dune systems. *Geomorphology*, *352*, 106995. https://doi.org/10.1016/j.geomorph.2019.106995
Jackson, D., Cruz-Avero, N., Smyth, T., & Hernández-Calvento, L. (2013). Three-dimensional airflow modeling and dune migration patterns in an arid coastal dune field. *Journal of Coastal Research*, *165*(65), 1301–1306. https://doi.org/10.2112/si65-220.1
Jackson, N. L., & Nordstrom, K. F. (2011). Aeolian sediment transport and landforms in managed coastal systems: A review. *Aeolian Research*, *3*(2), 181–196. https://doi.org/10.1016/j.aeolia.2011.03.011
Kaczkowski, H. L., Kana, T. W., Traynum, S. B., & Visser, R. (2018). Beach-fill equilibration and dune growth at two large-scale nourishment sites. *Ocean Dynamics*, *68*(9), 1191–1206. https://doi.org/10.1007/s10236-018-1176-2
Kana, T. W., & Kaczkowski, H. L. (2012). Planning, preliminary design, and initial performance of the Nags Head beach nourishment project. *Coastal Engineering Conference Proceedings*, *1*(33). https://doi.org/10.9753/icce.v33.sediment.109
Keijsers, J., Groot, A. D., & Riksen, M. (2015). Vegetation and sedimentation on coastal foredunes. *Geomorphology*, *228*, 723–734. https://doi.org/10.1016/j.geomorph.2014.10.027
Keijsers, J. G., Poortinga, A., Riksen, M. J., & Maroulis, J. (2014). Spatio-temporal variability in accretion and erosion of coastal foredunes in the Netherlands: Regional climate and local topography. *PLoS One*, *9*(3), e91115. https://doi.org/10.1371/journal.pone.0091115
Kratzmann, M. G., Himmelstoss, E. A., & Thieler, E. R. (2017). *National assessment of shoreline change—A GIS compilation of updated vector shorelines and associated shoreline change data for the southeast Atlantic coast*. U.S. Department of the Interior, U.S. Geological Survey. https://doi.org/10.5066/F74X55X7
Laporte-Fauret, Q., Marieu, V., Castelle, B., Michalet, R., Bujan, S., & Rosebery, D. (2019). Low-cost UAV for high-resolution and large-scale coastal dune change monitoring using photogrammetry. *Journal of Marine Science and Engineering*, *7*(3), 63. https://doi.org/10.3390/jmse7030063
Larson, M., Erikson, L., & Hanson, H. (2004). An analytical model to predict dune erosion due to wave impact. *Coastal Engineering*, *51*(8–9), 675–696. https://doi.org/10.1016/j.coastaleng.2004.07.003
Leaman, C., Beuzen, T., & Goldstein, E. B. (2020). *py-wave-runup v0.1.10*. Zenodo. https://doi.org/10.5281/zenodo.2667464
Levy, G. F. (1976). *Vegetative study at the Duck Field Research Facility, Duck, NC (Tech. Rep. No. 76-6)*. U.S. Army Corps of Engineers Coastal Engineering Research Center.
Lim, S., Thatcher, C. A., Brock, J. C., Kimbrow, D. R., Danielson, J. J., & Reynolds, B. (2013). Accuracy assessment of a mobile terrestrial lidar survey at Padre Island national seashore. *International Journal of Remote Sensing*, *34*(18), 6355–6366. https://doi.org/10.1080/01431161.2013.800658
Mathew, S., Davidson-Arnott, R., & Ollerhead, J. (2010). Evolution of a beach-dune system following a catastrophic storm overwash event: Greenwich dunes, Prince Edward Island, 1936–2005. *Canadian Journal of Earth Sciences*, *47*(3), 273–290. https://doi.org/10.1139/e09-078
McFall, B. C. (2019). The relationship between beach grain size and intertidal beach face slope. *Journal of Coastal Research*, *35*(5), 1080–1086. https://doi.org/10.2112/jcoastres-d-19-00004.1
Mendelssohn, I. A., Hester, M. W., Monteferrante, F. J., & Talbot, F. (1991). Experimental dune building and vegetative stabilization in a sand-deficient barrier island setting on the Louisiana coast, USA. *Journal of Coastal Research*, 137–149.
Miller, D. L., Thetford, M., & Yager, L. (2001). Evaluation of sand fence and vegetation for dune building following overwash by Hurricane Opal on Santa Rosa Island, Florida. *Journal of Coastal Research*, 936–948.
Morris, R. L., Konlechner, T. M., Ghisalberti, M., & Swearer, S. E. (2018). From grey to green: Efficacy of eco-engineering solutions for nature-based coastal defense. *Global Change Biology*, *24*(5), 1827–1842. https://doi.org/10.1111/gcb.14063
O'Dea, A., & Brodie, K. L. (2019). Spectral analysis of beach cusp evolution using 3D lidar scans. *Proceedings of the Coastal Sediments 2019 Conference*, 657–673.

Ollerhead, J., Davidson-Arnott, R., Walker, I. J., & Mathew, S. (2013). Annual to decadal morphodynamics of the foredune system at Greenwich Dunes, Prince Edward Island, Canada. *Earth Surface Processes and Landforms*, *38*(3), 284–298. https://doi.org/10.1002/esp.3327

Overbeck, J. R., Long, J. W., & Stockdon, H. F. (2017). Testing model parameters for wave-induced dune erosion using observations from hurricane sandy. *Geophysical Research Letters*, *44*(2), 937–945. https://doi.org/10.1002/2016gl071991

Palmsten, M. L., & Holman, R. A. (2012). Laboratory investigation of dune erosion using stereo video. *Coastal Engineering*, *60*, 123–135. https://doi.org/10.1016/j.coastaleng.2011.09.003

Reijers, V. C., Hoeks, S., van Belzen, J., Siteur, K., de Rond, A. J., van de Ven, C. N., et al. (2020). Sediment availability provokes a shift from Brownian to lévy-like clonal expansion in a dune building grass. *Ecology Letters*, *24*(2), 258–268. https://doi.org/10.1111/ele.13638

Renaud, A. D., Spore, N. J., Bruder, B. L., & Brodie, K. L. (2019). Lessons learned from coastal mapping efforts during the 2018 hurricane season using unmanned aerial systems (UAS) at Sandbridge, Virginia. (ERDC/CHL CHETN-IV-120).

Richter, A., Faust, D., & Maas, H.-G. (2013). Dune cliff erosion and beach width change at the northern and southern spits of Sylt detected with multi-temporal lidar. *Catena*, *103*, 103–111. https://doi.org/10.1016/j.catena.2011.02.007

Sallenger, A. (2000). Storm impact scale for barrier islands. *Journal of Coastal Research*, *16*(3), 890–895.

Sallenger, A., Stockdon, H., Haines, J., Krabill, W., Swift, R., & Brock, J. (2001). Probabilistic assessment of beach and dune changes. *Coastal Engineering Conference Proceedings*, *2000*, 3035–3047.

Schupp, C. A., McNinch, J. E., & List, J. H. (2006). Nearshore shore-oblique bars, gravel outcrops, and their correlation to shoreline change. *Marine Geology*, *233*(1–4), 63–79. https://doi.org/10.1016/j.margeo.2006.08.007

Sherman, D. J., & Hotta, S. (1990). Aeolian sediment transport: Theory and measurement. *Coastal Dunes: Form and Process*, *17*, 37.

Sherman, D. J., & Lyons, W. (1994). Beach-state controls on aeolian sand delivery to coastal dunes. *Physical Geography*, *15*(4), 381–395. https://doi.org/10.1080/02723646.1994.10642524

Short, A., & Hesp, P. A. (1982). Wave, beach, and dune interactions in southeastern Australia. *Marine Geology*, *48*(3–4), 259–284. https://doi.org/10.1016/0025-3227(82)90100-1

Sopkin, K. L., Stockdon, H. F., Doran, K. S., Plant, N. G., Morgan, K. L., Guy, K. K., & Smith, K. E. (2014). *Hurricane sandy: Observations and analysis of coastal change (No. Open-File Report 2014–1088)*. U.S. Geological Survey.

Spore, N. J., & Brodie, K. L. (2017). *Collection, processing, and accuracy of mobile terrestrial lidar survey data in the coastal environment (Tech. Rep.)*. U.S. Army Engineer Research and Development Center. (ERDC/CHL TR-17-5).

Stockdon, H. F., Holman, R. A., Howd, P. A., & Sallenger, A. (2006). Empirical parameterization of setup, swash, and runup. *Coastal Engineering*, *53*(7), 573–588. https://doi.org/10.1016/j.coastaleng.2005.12.005

Strypsteen, G., Houthuys, R., & Rauwoens, P. (2019). Dune volume changes at decadal timescales and its relation with potential aeolian transport. *Journal of Marine Science and Engineering*, *7*(10), 357. https://doi.org/10.3390/jmse7100357

Taddia, Y., Corbau, C., Zambello, E., & Pellegrinelli, A. (2019). UAVs for structure-from-motion coastal monitoring: A case study to assess the evolution of embryo dunes over a 2 yr time frame in the Po River Delta, Italy. *Sensors*, *19*(7), 1717. https://doi.org/10.3390/s19071717

van der Wal, D. (2000). Grain-size-selective aeolian sand transport on a nourished beach. *Journal of Coastal Research*, 896–908.

Vos, S., Lindenbergh, R., de Vries, S., Aagaard, T., Deigaard, R., & Fuhrman, D. (2017). Coastscan: Continuous monitoring of coastal change using terrestrial laser scanning. In *Proceeding of the Coastal Dynamics Conference* (pp. 1518–1528).

Walker, S. L., & Zinnert, J. (2022). Whole plant traits of coastal dune vegetation and implications for interactions with dune dynamics. *Ecosphere*, *13*(5), e4065. https://doi.org/10.1002/ecs2.4065

White, A. E. (2022). *Biotic characteristics of managed and unmanaged coastal dunes in the Outer Banks*. North CarolinaVirginia Commonwealth University. Retrieved from https://scholarscompass.vcu.edu/etd/7095/

Zarnetske, P. L., Hacker, S. D., Seabloom, E. W., Ruggiero, P., Killian, J. R., Maddux, T. B., & Cox, D. (2012). Biophysical feedback mediates effects of invasive grasses on coastal dune shape. *Ecology*, *93*(6), 1439–1450. https://doi.org/10.1890/11-1112.1